Blooming in a non-local, coupled phytoplankton-nutrient model

Veselic, V.

Viktoria Veselic

Blooming in a non-local, coupled phytoplankton-nutrient model

Master Thesis in Mathematics, 25th August 2011

Thesis advisor: Dr. V. Rottschäfer

Leiden University
Mathematical Institute

Contents

Chapter 1

Introduction

Phytoplankton is the collection of microscopic small plants that drift in the water columns of lakes, oceans, rivers. There exist many species of phytoplankton, approximately 5000, and new species are being discovered every day. Each phytoplankton species has its own characteristic shape, size, and features. Phytoplankton does not feed on any other organisms. Instead it depends on nutrients such as nitrate and phosphate, which are brought up by deep ocean currents. Phytoplankton forms the basis of nearly all food webs in aquatic ecosystems. Therefore it is vital to the health of all sorts of bodies of water. Through the process of photosynthesis, it converts carbon dioxide (CO_2) into oxygen and organic matter. Phytoplankton plays an important role in climate regulation because it extracts carbon dioxide from the atmosphere and transports significant amounts of carbon dioxide into the deep ocean. Phytoplankton is responsible for the production of most of the oxygen found in the Earth's atmosphere. Since phytoplankton depends on sunlight for photosynthesis and for their metabolism, it is usually found close to the surface, since light availability decreases rapidly with depth. Phytoplankton is confronted with contrasting gradients of two essential resources: light that is supplied from above and nutrients that are supplied from below. It is therefore not only important for phytoplankton to stay near the surface but it also has to be deep enough to get nutrients. Since phytoplankton depends on certain conditions for growth, such as nutrients and light, and because it is at the base of the aquatic food chain, it is a good indicator of changes in its environment. Phytoplankton populations respond rapidly to changes in their environment. Any decrease or increase in a population of phytoplankton due to changes in the environment, will most likely lead to changes in the populations of other types of aquatic life.

The dynamics of phytoplankton concentration in an ocean, lake or any other body of water, exhibits a variety of patterns. A phytoplankton concentration might become maximum at the bottom of a water column. This is called a benthic layer (BL). Or a phytoplankton concentration might become maximum

at the surface of a water column. This is called a surface layer (SL). Interesting patterns exhibited by phytoplankton are DCMs (deep chlorophyll maxima), in which the phytoplankton concentration has a maximum at a certain depth, far below the surface in the deep layers of an ocean or lake. The density of phytoplankton cells is a species-specific parameter and so is the vertical velocity V. Many phytoplankton species have a slightly higher density than water and therefore have an tendency to sink. For species heavier than water the vertical velocity V is positive and the motion is downwards. We refer to these species as sinking species. Some species have a lower density than water, for example due to a high oil content, they will float upwards. The vertical velocity V is negative and the motion is upwards. In this case the phytoplankton species will be called buoyant species.
In [17] a non-local, coupled phytoplankton-nutrient model was studied for a sinking species. In this model an equation for a phytoplankton concentration W is coupled to an equation for a nutrient N. This model is based on the model in [10], where it is shown that such systems may exhibit complex behaviour ranging from periodically oscillating DCMs to chaotic DCMs. The model in [17] was studied for sinking species, to understand the bifurcational structure associated to such models. For sinking species, the mathematical analysis predicts for any given values of the parameters whether one may expect a phytoplankton pattern with the structure of a (possibly oscillating) DCM, a pattern with the structure of a BL, or whether the phytoplankton will become extinct. The **topic** of this thesis is to determine the structure of phytoplankton patterns that are exhibited by buoyant species. For any given value of parameters we want to be able to predict the structures of the phytoplankton patterns for buoyant species. To determine the bifurcational structure associated to the model for buoyant species, we have studied the model from [17]. But now with $V < 0$ instead of $V > 0$. All the mathematical analysis in this thesis has been performed for $V < 0$ and for $V > 0$. In every chapter the results for the sinking species are also stated and explained. In every chapter it is also made clear which results were found in [17] and which results were found in this thesis.

We now present the outline of the chapters. In chapter 2 we give background information of phytoplankton. In chapter 3 we explain what a DCM is, and we give a summary of the results in [10]. In chapter 4 we introduce and motivate the non-local, coupled phytoplankton-nutrient model for one phytoplankton species from [17]. First, we scale the model into a system with a natural singularly perturbed nature. Then, we will determine the the associated eigenvalue problem, which can be decoupled into a problem of Sturm-Liouville type. Therefore it is possible to obtain explicit (and rigorous) bounds on, and accurate approximations of, the eigenvalues. These bounds on the eigenvalues are stated in the main result Theorem 5.1 in chapter 5. In this chapter we also summarise the outcome of [17] and the outcome of this thesis. That is, for the eigenfunction we give the structures of the phytoplankton species that corresponds to the profiles. We use two different analytical approaches to study the structure of the eigen-

value problem. In chapters 6 and 7 we derive explicit and rigorous bounds on the eigenvalues in terms of expressions based on the zeros of the Airy functions of the first kind and its derivatives. In chapter 8 we derive eigenfunctions for the eigenvalues for the buoyant species. We also describe the profiles of these eigenfunctions. The detailed knowledge of the eigenvalues and eigenfunctions of the Sturm-Liouville problem forms the foundation of analytical insight in the bifurcations exhibited by the rescaled model. The analysis of the Sturm-Liouville problem is completed by a WKB approach in chapter 9. Using this method we deduce for buoyant species the structures of the phytoplankton patterns corresponding to the critical eigenfunctions. We determine the structures of the phytoplankton concentrations that correspond to the profiles of the eigenfunctions. In chapter 10 we determine the bifurcation curves in the biological parameter space associated to the model, for buoyant species. As in [17], the mathematical analysis predicts, for any given values of parameters, the structure of the phytoplankton pattern. In chapter 11 we explain the limitations of the model. Chapter 12 contains summary and conclusion.

Chapter 2

Phytoplankton

2.1 General features of phytoplankton

Phytoplankton is the collective of microscopic, photosynthetic organism that live suspended in seas, lakes, ponds, and rivers. The word phytoplankton comes from the Greek words for "plant" and "floating". Phytoplankton are for example algae, bacteria, viruses. It is important to realize the diversity among phytoplankton. Approximately between 4000 and 5000 species of marine phytoplankton have been described and new species are being discovered all the time. The first phytoplankton existed approximately 3 billion years ago.

Through the process of **photosynthesis** phytoplankton converts inorganic material into new organic compounds using the energy from the sun. This process is very complex and consists of a series of reactions. These chemical reactions can be generally summarized as:

$$6CO_2 \ + \ 6H_2O \ \longrightarrow \ C_6H_{12}O_6 \ + \ 6O_2$$

Phytoplankton is an **autotrophic** organism, that is, it does not require organic materials as an energy source. The primarily nutrients are nitrate (NO_3^-), phosphate (PO_4^{3-}) and silicic acid (SiO_2). Since phytoplankton needs photosynthesis to grow, it lives in the sunlit surface waters of the **euphotic zone**. This zone includes the surface waters of the oceans, where light is sufficient to support photosynthesis, and therefore support the growth and reproduction of plants. Phytoplankton is present throughout the lighted regions of all seas, including under ice in polar regions.

Phytoplankton is the dominant **primary producer** of the pelagic realm, building organic material from inorganic elements by the process of photosynthesis,

and thereby starting the pelagic food chain. The pelagic realm is that of the ocean water column, from the surface to the great depths. Because it is at the base of the aquatic food web, it provides an essential ecological function for all aquatic life.

Respiration is essentially the reverse reaction of photosynthesis. It is a metabolic process, in which organic substances are broken down and as an consequence the energy stored in organic matter is released. The result of respiration is that a part of the CO_2 taken up by phytoplankton is released back into the atmosphere. The other part becomes incorporated into plant tissue. The chemical reactions for respiration can be generally summarized as:

$$C_6H_{12}O_6 + 6O_2 \longrightarrow 6CO_2 + 6H_2O + \text{energy}$$

All organisms, including plants, carry out respiration. In contrast to photosynthesis, respiration is carried out during both light and dark periods.

The conversion of radiant energy to chemical energy during the process of photosynthesis depends on special photosynthetic pigments such as **chlorophyll** and **accessory pigments**. These photosynthetic pigments are usually contained in the chloroplasts of the algae. Chlorophyll is a group of green plant pigments that capture photons of light that are used in photosynthesis. Among these pigments, the dominant pigment is chlorophyll *a*, but there are many other pigments present. There are also accessory pigments, these are plant pigments other than chlorophyll that capture photons of light used in photosynthesis, such as carotenes. A phytoplankton **bloom** is the sudden appearance of a high concentration phytoplankton which is a result of an increased reproduction of a species as a response to favourable conditions. When these accessory pigments dominate over the green colour of chlorophyll the colour of the water turns red or brown.

2.2 Water and phytoplankton

Phytoplankton is by no means a simple organism. The relationship that phytoplankton has with the physical properties of its environment is very complex. It is important to notice that water is a very important component which needs to be taken in account. Water has very special properties, it is relatively dense, viscous and a barely compressible fluid. This means for phytoplankton species that they live in an environment that is characteristically viscous. Water is always in motion and the movement of water is, almost always, turbulent. That is, the flow is not along trajectories but in billowing **eddies** or **gyres**, which are small respectively large circular movements of water. **Turbulence** is the physical mixing of water, and is due to wind, currents, eddies, and gyres. Oceanic

surface currents generated by global wind systems, and their direction is modified by the Earth's rotation. This results in gyres, large circular movements of water, in the oceans.

A vital requirement for all phytoplankton species is to stay in the upper well lit layer at most times. Its intrinsic movements are to weak to overcome the velocity and direction of all possible movements in the water. Because phytoplankton species only seldomly have the same density as water, they have a tendency either to float upwards or sink downwards. Physical mixing mechanisms create the required turbulence to keep populations suspended in the water column. These mechanisms also govern the degree of turbulence in the phytoplankton's environment. All these movements in the water influence the velocity and direction of the settling phytoplankton. To counteract the inevitability of sinking, different species of phytoplankton have very different sophisticated means and adaptive strategies of overcoming the problems in all sorts of water and remaining in the water column. For example, certain species can regulate their cell density and buoyancy, and therefore position themselves in the most favourable light and nutrient conditions. Settling can also be controlled by altering shape while density and volume remain constant. There exists an enormous diversity in size and shape, factors that have a significant influence on the sinking rates.

2.3 Growth of phytoplankton

There are many different variables that limit the growth of phytoplankton, which is primarily reliant on nutrient supply, light availability and temperature. All these variables are constantly changing. Nutrients concentrations vary constantly, light and temperature change daily and seasonally. There are also other physical properties such as salinity, wind conditions, turbulence, that influence the growth of phytoplankton. The amount of nutrients and light an algae cell receives depends on its position in the water column, which is in part controlled by mixing and circulation.
Mortality is also a factor that influences phytoplankton concentration. Mortality reduces phytoplankton concentration and is due to a variety of causes: not enough light and nutrient concentration needed for production, unsuitable temperatures, disease and infection by viruses, or grazing by higher order organisms.
Long term temporal changes may also have an effect on phytoplankton dynamics: changes in climate, pollution, fishery.
All the mentioned processes and factors that influence the concentration of phytoplankton are subject to strong changes in season, and differ from place to place. This means that the primary productivity in phytoplankton in various areas of the global ocean varies with season and location.

Each species responds differently to these constantly changing conditions in their environment. Every phytoplankton species has its own optimal growth rate, which is highly influenced by temperature. All phytoplankton species have different nutrient concentrations requirements and favour different light conditions. Because different species of phytoplankton respond differently to changes in their environment, changing environmental conditions will favour different species at different times. These species-specific differences in growth rates and responses to nutrients allows for the coexistence of many species in the same body of water. As a result, there are different species at different times and this leads to a succession of different dominant species in the community.

The well illuminated surface layer is generally depleted of nutrients while little light reaches deeper waters which are rich in nutrients. As a consequence, it is necessary for phytoplankton, that there is a compromise between being deep enough to be able to get higher nutrient availability, but shallow enough to be able to harvest enough light for photosynthesis.

2.4 Phytoplankton and the carbon cycle

The fixation of carbon by primary producers, mainly plants, is the basis of all life on Earth. In the global carbon cycle, carbon is continually cycled through all sorts of reservoirs such as: Earth's living organisms, the soil, the atmosphere, and the oceans. The element carbon moves periodically between these reservoirs and rearranges itself into different compounds. The carbon cycle involves cycling from timescales of years or decades, up to hundreds of thousands of years. The overall carbon cycle is actually a number of cycles that occur on these different timescales. These cycles link these different timescales together.
In the oceanic carbon cycle the organic matter in dead phytoplankton cells and animal's fecal material sinks and is consumed by microbes. These microbes convert it back into inorganic nutrients, including CO_2. Much of this recycling happens in the sunlit layer of the ocean, where the CO_2 is instantly available to be photosynthesized or absorbed back into the atmosphere. A major part of the organic matter is decomposed during sinking and can be returned to the surface by upwelling of deep water. However another part of the organic matter, that sinks before it decays or is being eaten, is stored into the deep ocean. The biological process, in which phytoplankton removes CO_2 from the surface waters and atmosphere and stores it in the deep ocean is called the **biological pump**. The result is a storage of carbon for periods of decades to centuries or even permanently in the sediments. Permanent storage may be in the form of organic matter, the type material that is the source of oil and natural gas. Fossil fuels are ancient deposits of organic matter that have transformed into oil, natural gas, or coal.
It is necessary to understand how the biological pump varies both geograph-

ically and temporally to predict CO_2 concentrations in the atmosphere. It is also important to understand the effects that changes in temperature, ocean circulation and ocean chemistry have on the biological pump.

2.5 Studying phytoplankton

As described in the introduction, phytoplankton depends on sunlight, water, and nutrients to survive. Physical or chemical changes in any of these ingredients will affect a phytoplankton population for a given region. Phytoplankton populations will grow or diminish rapidly in response to changes in their environment. On the other hand, changes in a population is a sign that environmental conditions are changing in that region. By measuring these changes in populations and comparing them to other measurements, such as temperature, we can learn more about how phytoplankton may be contributing to environmental changes and climate changes. And also how it is affected by changes in the climate and environment.

Phytoplankton populations are observed with satellite instruments. All phytoplankton have chlorophyll *a* and accessory pigments. These pigments absorb the blue and green wavelengths of sunlight, whereas water molecules scatter them. Depending on the type and density of the phytoplankton population, the ocean over regions with high concentrations of phytoplankton will appear blue, green or green-blue. The more phytoplankton absorbs sunlight in a given area, the darker that part of the ocean looks to an observer from space. A satellite detects different concentrations of chlorophyll *a*. Satellite measurements of the ratio of blue-green light leaving the ocean is thus a way to quantify chlorophyll, and thus a way to measure phytoplankton abundance. The reason that changes in populations of phytoplankton can be easily observed using satellite images is due to the rapid life cycle of phytoplankton. Phytoplankton increases its population very fast but lives only a short time. Phytoplankton cells divide - every six days on average - half the daughter cell die or are eaten by zooplankton, that in turn provide food for shrimps, fish and larger carnivores. In contrast, land plants must invest huge amounts of energy to build wood, leaves and roots and take an average of twenty years to replace themselves. It would therefore not be so easy to observe the changes in productivity of a forest of long-lived trees. Satellite analysis reveals that phytoplankton draw nearly as much CO_2 out of the atmosphere and oceans through photosynthesis as do trees, grasses and all other plants combined.
Also long-term sampling programs are being used to study phytoplankton. Phytoplankton samples are taken to see how it is affected by the physical environment and its food web interactions. The satellite images of chlorophyll, together with thousands of productivity measurements, and mathematical models has contributed to our knowledge about phytoplankton and its environment.

Chapter 3

Oscillations and chaos in the oceanic deep chlorophyll maximum

In chapter 2 we have explained the different phytoplankton patterns that can be a found in an ocean, lake or in an other body of water. In this chapter we explain in more detail what a DCM exactly is. By studying this pattern, we will get a better understanding of phytoplankton dynamics. This chapter is a summary of [10], where it was shown that DCMs are not always stable features but can also show sustained fluctuations. These are caused by a difference in the timescales of two processes. The first process is the rapid export of sinking phytoplankton withdrawing nutrients from the euphotic zone. The second process is a slow upward flux of nutrients needed for new phytoplankton production. The model in [10] shows that reduced vertical mixing can generate oscillations and chaos in phytoplankton biomass and species composition of DCMs. This variability in DCMs enhances the variability in oceanic primary production and in carbon export into the oceanic interior.

We start this chapter by giving the definition of a DCM. In section 2.2 we introduce the model and explain what exactly happens to a phytoplankton population in a DCM when turbulent diffusivity is reduced. In section 2.3 we give a summary of the model's predictions.

3.1 The definition of a DCM

Deep chlorophyll maxima (DCM) are absolute maxima of chlorophyll *a* concentration that can be found in deep layers far from the surface. In other words, a

DCM is a presence in high concentrations of chlorophyll far beneath the surface. They are widespread in large parts of the world's oceans and in lakes. There are many possible mechanisms that are responsible for the formation of a particular DCM which we will not be explaining here. A DCM is formed by only a few phytoplankton species. The species that form DCMs have the ability to cope with the special environmental features at these depths. They can accumulate dense populations at depths where there is low light availability and where nutrient limitation can be less severe.
DCMs are often found in oligotrophic waters, where the surface mixed layer is depleted of nutrients, and they generally develop in the metalimnion of a stratified water body. Stratification is the separation of water into layers based on density differences. The metalimnion is the middle layer of a stratified water body. It is the region with the most prominent temperature, oxygen, nutrient and density gradients. DCMs are permanent features in large parts of the tropical and subtropical oceans (Fig. 3.1a,b).

3.2 Oscillations and chaos in a DCM

We now introduce the partial differential equations of the model that was used in [10] to study the various phytoplankton patterns that can occur. This model will be explained in full detail in chapter 4. The model in [10] has as extra term, the term recycling, in the partial differential equation $\frac{\partial N}{\partial t}$. This term is not included in [17] and in this thesis. For now it suffices to see and understand the terms of the partial differential equations. Let W denote the phytoplankton population density, that is the number of cells per m^3. Then the population dynamics of the phytoplankton can be described by the following partial differential equation

$$\begin{aligned} \frac{\partial W}{\partial t} &= \text{growth} - \text{loss} - \text{sinking} + \text{mixing} \\ &= \mu P(L,N)W - lW - VW_z + DW_{zz} \end{aligned}$$

Let N denote a nutrient. Then the nutrient dynamics can be described by the partial differential equation

$$\begin{aligned} \frac{\partial N}{\partial t} &= -\text{uptake} + \text{recycling} + \text{mixing} \\ &= \alpha\mu P(L,N)W + \varepsilon\alpha lW + DN_{zz} \end{aligned}$$

It is often argued that DCMs are stable features. A DCM is stable if the population settles at a stable equilibrium at which the downward flux of consumed nutrients equals the upward flux of new nutrients (Fig. 3.2a). However, the

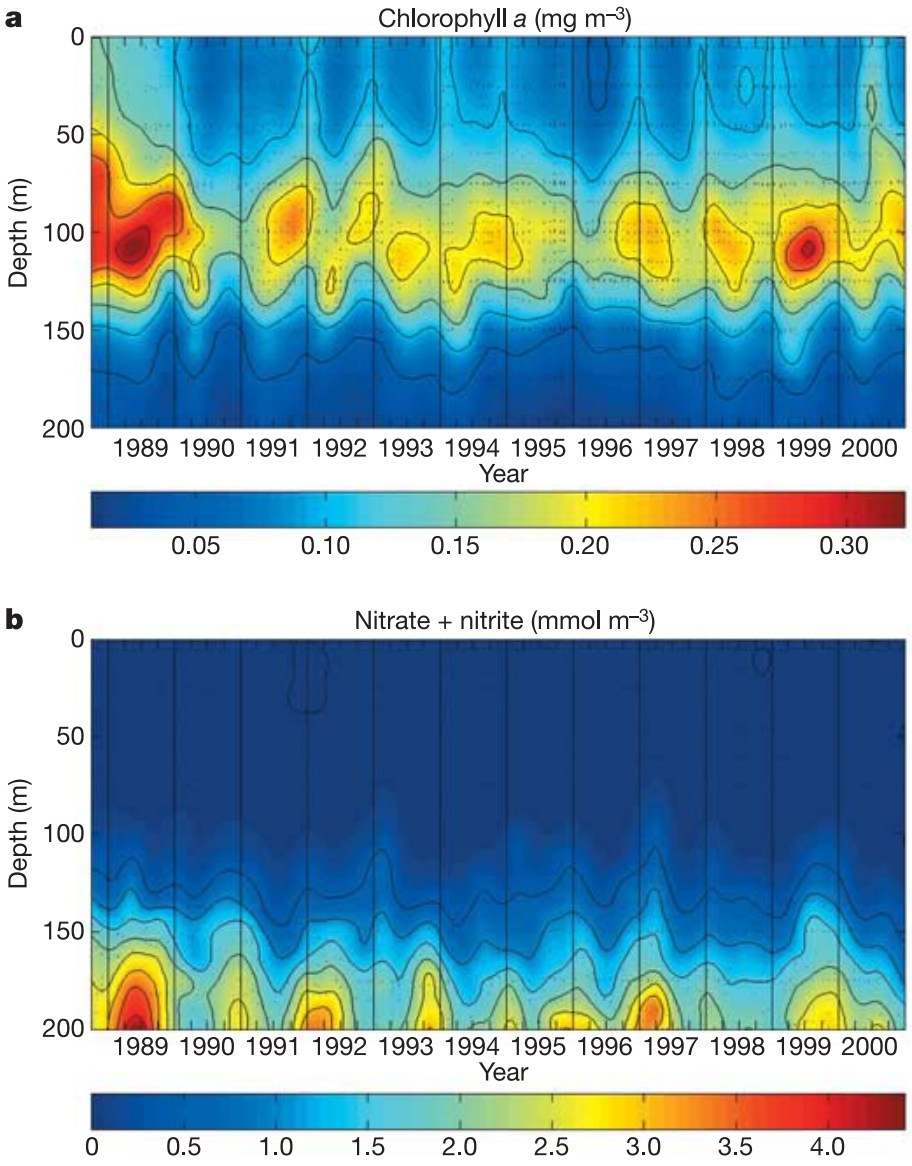

Figure 3.1: **Time course of the DCM at Station ALOHA, in the subtropical Pacific Ocean, North of Hawaii. a.** *Clorophyll a* **b.** Nitrate and nitrite.

model predicts that if vertical mixing is reduced, the phytoplankton population in the DCM will oscillate. This phenomenon was investigated by running numerous simulations using a wide variety of turbulent diffusivities. Depending on the parameter settings, fluctuations in the DCM can range from mild oscillations (Fig. 3.2b) to pronounced chlorophyll peaks (Fig. 3.2c).

The model also shows that fluctuating DCMs show even more complex dynamics in a seasonal environment than in a constant environment. In a seasonal environment, there are seasonal changes in light conditions which have a large effect on the dynamics of DCMs. Seasonal DCMs commonly develop in temperate regions and even in polar oceans. In a model simulation with turbulent diffusivity of $0.50\text{cm}^2\text{s}^{-1}$, the DCM tracks the seasonal changes in light (Fig. 3.2d). For lower values of turbulent diffusivities the model predicts that the DCM shows double periodicity (Fig. 3.2e). For even more lower values of turbulent diffusivity, seasonal forcing generates irregular phytoplankton blooms with chaotic multi-annual variability (Fig. 3.2f).

These fluctuations in the DCM are caused by a difference in the timescale between the sinking flux of phytoplankton and the upward diffusive flux of nutrients. Model simulations indicate that the sinking flux has an important role in these oscillations, as oscillations were not observed with neutrally buoyant species.
The model simulations predict that for very low values of turbulent diffusivity the DCM becomes unstable, and a chaotic DCM can develop (Fig. 3.3.a,b). The period and amplitude of the DCM oscillations increase with increasing phytoplankton sinking velocity (Fig. 3.3c), and they decrease with increasing vertical diffusivity (Fig. 3.3d). Thus, the model shows that oscillations become more pronounced if the timescale of sinking is fast compared to the timescale of the upward flux of nutrients.

In reality, DCMs consist of multiple phytoplankton species with different growth rates, nutrient and light requirements, and sinking velocities. In order to find out how such a diverse assemblage would respond to fluctuations in the DCM, a multi-species version of the DCM model in [17] was developed. This multi-species DCM model is analogous to earlier phytoplankton competition models, and is also forced by seasonal changes in incident light intensity (Fig. 3.4). Periods with co-dominance are altered with periods in which one of the three species dominate (Fig. 3.4e). Simulations show that all three species persist in a non-equilibrium environment, which confirms earlier notions that oscillations and chaos promote phytoplankton diversity.

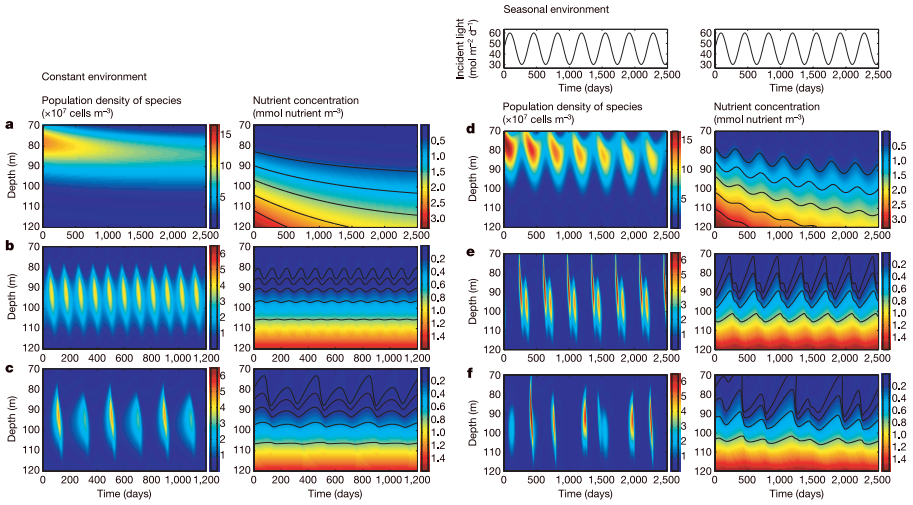

Figure 3.2: **Model simulations at different intensities of vertical mixing.** For **a-f**, the left panel shows phytoplankton dynamics (P) and the right panel shows nutrient dynamics (N).
a-c. Constant environment.
a. Stable DCM ($\kappa = 0.50$ cm^{2}s^{-1}).
b. Mild oscillations in the DCM ($\kappa = 0.20$ cm^{2}s^{-1}).
c. Large-amplitude oscillations in the DCM, double periodicity ($\kappa = 0.12$ cm^{2}s^{-1}).
d-f. Seasonal environment in which the model is forced by seasonal changes in incident light itensity.
d. DCM tracks seasonal variability ($\kappa = 0.50$ cm^{2}s^{-1}).
e. Double periodicity of DCM locked in a seasonal environment ($\kappa = 0.14$ cm^{2}s^{-1}).
f. Chaotic DCM in a seasonal environment ($\kappa = 0.08$ cm^{2}s^{-1}).

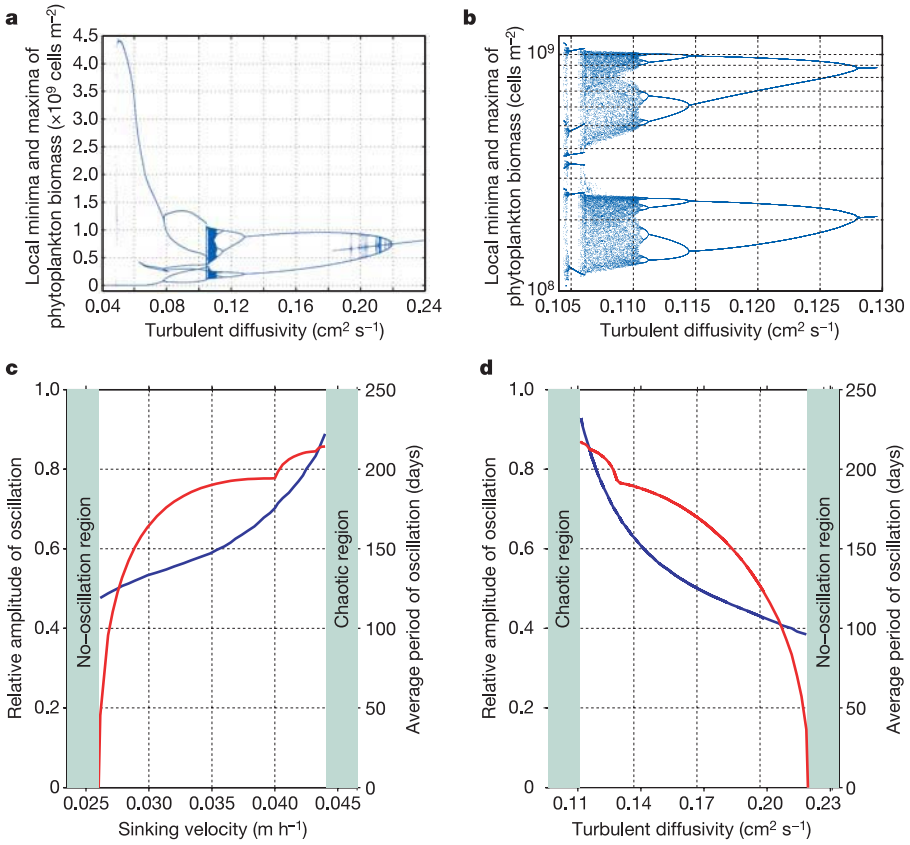

Figure 3.3: **Bifurcation Patterns generated in a constant environment.**
a. Bifurcation diagram showing the local minima and maxima of the phytoplankton population as a function of turbulent diffusivity.
b. Detail of the chaotic region in the bifurcation diagram.
c. The period (blue line) and relative amplitude (red line) of the oscillations increase with phytoplankton sinking velocity.
d. The period (blue line) and relative amplitude (red line)of the oscillation decrease with vertical turbulent diffusivity.

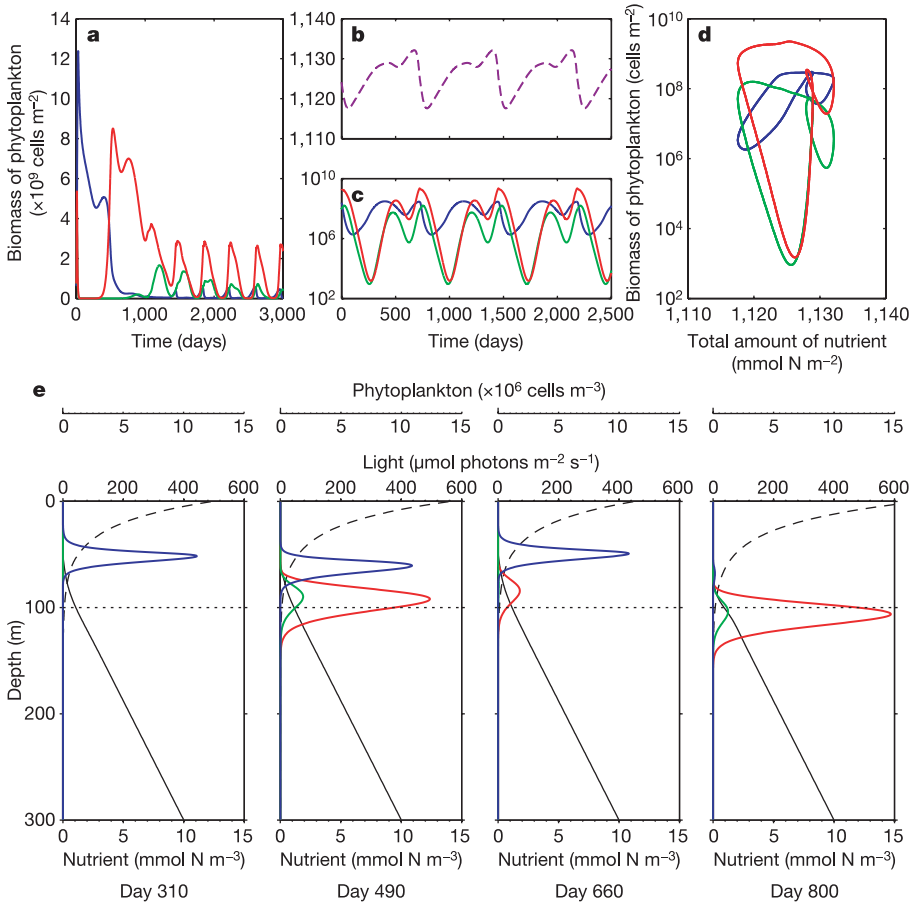

Figure 3.4: **Competition between three phytoplankton species in an oscillating DCM.**
The model (with $\kappa = 0.12$ cm^{2}s^{-1}) is forced by the same seasonal changes in incident light itensity as in Fig. **2d-f**.
a. Initial time course of the phytoplankton species.
b,c. In the long run, the nutrient concentration (**b**) and the phytoplankton concentration (**c**) settle down at a periodic attractor.
d. Phase plane illustrating the periodic attractor of the phytoplankton species.
e. Time series of of consecutive depth profiles within a single period. Coloured lines show depth profiles of the three phytoplankton species, dashed lines shows light intensity, black lines show nutrient concentration.
In **a-d** phytoplankton population density and nutrient concentration are integrated over the upper 300 m of the water column.

3.3 The model's predictions

The model is parameterized for clear ocean water, reflecting the North Pacific subtropical gyre. Although this model is a simple version of the reality, it reproduces many features of real-world DCMs. We give a summary of the predictions of this model. As stated before this model predicts that the process of reduced vertical mixing may induce oscillations and chaos in the phytoplankton of the DCM, generated by the difference in timescale between the sinking flux of phytoplankton and the upward flux of nutrients. Other predictions of the model are

1. DCMs form at a similar depth of 100m and span a similar depth range as observed in clear ocean waters.
2. These ocean time series confirm the prediction that the seasonal light cycle gives rise to seasonal patterns in chlorophyll and nutrient concentrations in the DCM (Fig. 3.1).
3. Detailed ocean measurements from the subtropical North Pacific confirm the prediction of a vertical zonation of species, with different species assemblages dominating at different depths.
4. The time series tentatively suggest that phytoplankton species with relatively high sinking velocities show larger variability than small phytoplankton species with low sinking velocities (Fig. 3.4c-e).

In total, time-series data support the theoretical prediction that deep chlorophyll maxima can show sustained non-equilibrium dynamics, driven by a combination of external forces and the complex internal dynamics of DCMs.

Chapter 4

A phytoplankton-nutrient model

In this chapter we introduce and motivate our model in which a phytoplankton concentration W is coupled to an equation for a nutrient N. This model was used in [17] for sinking species, to understand the bifurcational structure of non-local, coupled phytoplankton-nutrient models. In this thesis we use exactly the same model, this means that we use the same partial differential equations, functions, and boundary conditions. As stated in the introduction, all the analysis in this thesis was done for the sinking species with $V > 0$, and then again for the buoyant species with $V < 0$. We are especially interested in the results of the analysis for the buoyant species.
In the first section we introduce and explain all the parameters and the functions of the model. In section 4.2 we rescale the model obtaining dimensionless variables which we will use in the analysis. In section 4.3 we determine the one component Sturm-Liouville problem.

4.1 The model

We consider the one-dimensional, i.e. depth-dependent only, non-local model. In this model the phytoplankton concentration W is coupled to an equation for nutrients N. Let z denote the depth within the water column, where z runs from 0 at the top to a (maximum) depth, z_m, at the bottom. And let W denote the phytoplankton population density (number of cells per m^3 at time t and depth z). We consider the one-dimensional, non-local model

$$\begin{cases} W_t &= DW_{zz} - VW_z + [\mu P(L,N) - l]W, \\ N_t &= DN_{zz} - \alpha\mu P(L,N)W. \end{cases} \tag{4.1}$$

for $(z,t) \in \mathbf{R}_+$ and z is positive downwards. Here D is the diffusion coefficient, V is the sinking speed of phytoplankton, l is the species-specific loss rate, α is the conversion factor and μ is the maximum specific production rate. The parameters l, α, and μ are all assumed to be positive. The velocity V for the sinking specie is positive and downwards, for the buoyant species it is negative and upwards.

The light intensity L is modeled by

$$L(z,t) = L_I e^{-K_{bg}z - R\int_0^z W(\zeta,t)d\zeta}, \tag{4.2}$$

where L_I is the intensity of light at the water surface. We assume that the light intensity decreases exponentially with depth following Lambert-Beer's law. Light is absorbed by the phytoplankton population, by water and by dissolved substances. K_{bg}, R are the light absorption coefficients due to non-plankton components and due to the plankton respectively.

The function $P(L,N)$ is responsible for the coupling and models the influence of light and nutrient on the phytoplankton growth

$$P(L,N) = \frac{LN}{(L+L_H)(N+N_H)}, \tag{4.3}$$

where L_H and N_H are half-saturation constants of light and nutrient, respectively.

We assume zero-flux boundary conditions

$$\begin{aligned} DW_z - VW = 0, \quad \text{at} \quad z = 0 \quad \text{and} \quad z = z_B, \\ N_z = 0 \quad \text{at} \quad z = 0, \quad \text{and} \quad N = N_B \quad \text{at} \quad z = z_B. \end{aligned} \tag{4.4}$$

That is, phytoplankton does not enter or leave the water column neither at the top nor at the bottom. Nutrients do not leave the top of the water column but are supplied at the bottom, where N takes its maximum.

4.2 Rescaling the model

We recast the model in non-dimensional variables by rescaling time and space

$$x = z/z_B \in (0,1) \quad \text{and} \quad \tau = \mu t \geq 0.$$

We also introduce the scaled phytoplankton concentration ω, nutrient concentration η and light intensity j

$$\omega(x,\tau) = \frac{l\alpha z_B^2}{DN_B} W(z,t), \quad \eta(x,\tau) = \frac{N(z,t)}{N_B}, \quad j(x,t) = \frac{L(z,t)}{L_I}.$$

Recasting (4.1) we obtain the following form

$$\left\{ \begin{array}{rcl} \omega_\tau & = & \varepsilon\omega_{xx} - \sqrt{\epsilon}a\omega_x + (p(j,\eta) - \ell)\omega, \\ \eta_\tau & = & \varepsilon(\eta_{xx} - \frac{1}{\ell}p(j,\eta)\omega). \end{array} \right. \tag{4.5}$$

Here,

$$j(x,\tau) = \exp(-\kappa x - r\int_0^x \omega(\chi,\tau)d\chi), \quad \text{with} \quad \kappa = K_{bg}z_B \quad \text{and} \quad r = \frac{RDN_B}{l\alpha z_B}, \tag{4.6}$$

and

$$\varepsilon = \frac{D}{\mu z_B^2}, \quad a = \frac{V}{\sqrt{\mu D}}, \quad \ell = \frac{l}{\mu} \quad \text{and} \quad p(j,\eta) = \frac{j\eta}{(j+j_H)(\eta+\eta_H)}, \tag{4.7}$$

where

$$j_H = L_H/L_I, \quad \eta_H = N_H/N_B.$$

The rescaled conditions are given by

$$(\sqrt{\varepsilon}\omega_x - a\omega)(0) = (\sqrt{\varepsilon}\omega_x - a\omega)(1) = 0, \quad \eta_x(0) = 0 \quad \text{and} \quad \eta(1) = 1. \tag{4.8}$$

The scalings are suggested by realistic parameter values in the original model (4.1) as reported in [17]. Typically, we might have

$$D \approx 0.1\ cm^2/s, \quad V \approx 4.2\ cm/h, \quad z_B \approx 3 \cdot 10^4\ cm, \quad l \approx 0.01/h \quad \mu \approx 0.04/h,$$

so that

$$\varepsilon \approx 10^{-5}, \quad a \approx 1 \quad \text{and} \quad \ell \approx 0.25 \tag{4.9}$$

in (4.5). Thus realistic choices of the parameters in (4.1) induce a *natural singularly perturbed structure* in the model, as is made explicitly by the scaling of (4.1) into (4.5). In this article, ε shall be considered as an asymptotically small parameter, i.e. $0 < \varepsilon \ll 1$.

4.3 The Sturm-Liouville problem

The simulations in [17] indicate that the DCMs bifurcate from the trivial stationary pattern,

$$\bar{\omega}(x,\tau) \equiv 0, \quad \bar{\eta}(x,\tau) \equiv 1, \quad \text{for all} \quad (x,\tau) \in [0,1] \times \mathbf{R}_+ \tag{4.10}$$

To analyze this first bifurcation, we set

$$(\omega(x,\tau), \eta(x,\tau)) = (\tilde{\omega} e^{\lambda\tau}, 1 + \tilde{\eta} e^{\lambda\tau}), \quad \text{with} \quad \lambda \in \mathbf{C},$$

and consider the spectral stability of $(\bar{\omega}, \bar{\eta})$. This yields the linear eigenvalue problem,

$$\left\{ \begin{array}{rcl} \varepsilon\omega_{xx} - \sqrt{\varepsilon} a \omega_x + (f(x) - \ell)\omega & = & \lambda\omega \\ \varepsilon(\eta_{xx} - \frac{1}{\ell} f(x)\omega) & = & \lambda\eta, \end{array} \right. \tag{4.11}$$

where the tildes have been dropped. The linearized boundary conditions here are also given by (4.8), while the function f is the linearization of the function $p(j,\eta)$

$$f(x) = \frac{1}{(1+\eta_H)(1+j_H e^{\kappa x})} \tag{4.12}$$

The linearized system (4.11) is partially decoupled, so that the stability of $(\bar{\omega}, \bar{\eta})$ as the solution of the two-component system (4.1) is determined by a one-component Sturm-Liouville problem,

$$\begin{aligned} \varepsilon\omega_{xx} - \sqrt{\varepsilon}a\omega_x + (f(x) - \ell)\omega &= \lambda\omega \qquad (4.13) \\ (\sqrt{\varepsilon}\omega_x - a\omega)(0) = (\sqrt{\varepsilon}\omega_x - a\omega)(1) &= 0. \end{aligned}$$

Chapter 5

The main results

In this section we will introduce the main result Theorem 5.1 which was derived in [17]. This Theorem is also valid buoyant species. Before introducing the theorem, we define a number of functions which we will be using throughout the whole work. Then, we explain the facts that are established by the theorem. Finally we give a summary of the results of the analysis of [17] for the sinking species ($a > 0$), and also the main results for the buoyant species ($a < 0$) found in this thesis.

First, we define the function F through

$$F(x) = F(x; j_H, \kappa, \eta_H) = f(0) - f(x) \geq 0 \quad \text{for all} \quad x \in [0, 1] \tag{5.1}$$

see (4.12), and the constants $\sigma_L = \sigma_L(\kappa, j_H, \eta_H)$ and $\sigma_U = \sigma_U(\kappa, j_H, \eta_H)$ so that

$$\sigma_L x \leq F(x) \leq \sigma_U x, \quad \text{for all} \quad x \in [0, 1] \tag{5.2}$$

The optimal values of σ_U and σ_L can be determined explicitly. This is stated in Lemma 5.1 at the end of this section.

We write Ai and Bi for the Airy functions of the first and second kind, respectively, and $\mathrm{A_n} < 0$ for the n-th zero of $\mathrm{Ai}(x)$.

We also define the functions

$$\begin{aligned} \Gamma(\mathrm{Ai}, x) &= \mathrm{Ai}(x) - 2\varepsilon^{1/6}\sigma^{1/3}a^{-1}\mathrm{Ai}'(x) \\ \Gamma(\mathrm{Bi}, x) &= \mathrm{Bi}(x) - 2\varepsilon^{1/6}\sigma^{1/3}a^{-1}\mathrm{Bi}'(x), \end{aligned} \tag{5.3}$$

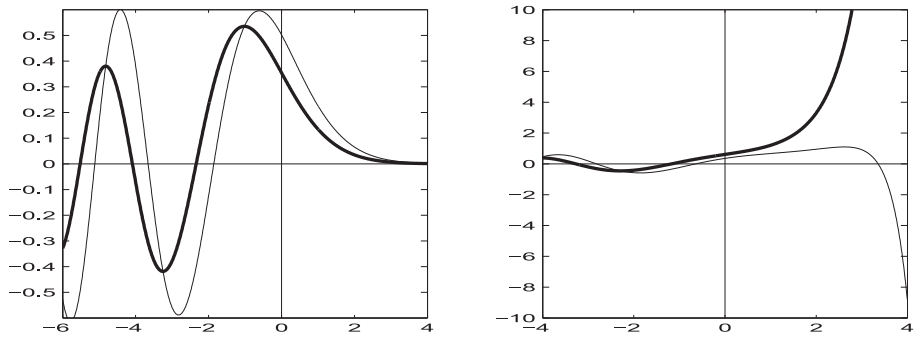

Figure 5.1: The Airy functions of first and second kind (plotted in thick lines in the left and right panel, respectively) together with the functions $\Gamma(\mathrm{A_i}, x)$ and $\Gamma(\mathrm{B_i}, x)$ (plotted in thin lines). Here, $\varepsilon = 0.1$, $a = 3$, $\sigma = 2$.

with a as in (4.7) and σ an *a priori* parameter. This parameter will later be set to σ_L or σ_U.

We let $A'_{n,\sigma}$, $n = 1, 2, \ldots$, be the $n-$th zero of $\Gamma(\mathrm{Ai}, x)$ and $B_{0,\sigma}$ be the positive zero of $\Gamma(\mathrm{Bi}, \varepsilon^{-1/3}\sigma^{1/3}(1+x))$. Note that $A'_{n,\sigma}$ is $\mathcal{O}(\varepsilon^{1/6})$ close to A_n and that $B_{0,\sigma} = a^2/4\sigma - 1$ at leading order in ε. See Lemma A.2 for more accurate estimates.

Finally, we let

$$\begin{aligned} \lambda^* &= f(0) - \ell - a^2/4, \\ \lambda_0^{*,\sigma} &= \lambda^* + \sigma B_{0,\sigma}, \\ \lambda_n^{*,\sigma} &= \lambda^* - \varepsilon^{1/3}\sigma^{2/3}|A'_{n,\sigma}|, \end{aligned} \tag{5.4}$$

where $n \in \mathbf{N}$ and we note that $\lambda_0^{*,\sigma}$ and $\lambda_n^{*,\sigma}$ are decreasing functions of σ.

Now we can state the main result.

Theorem 5.1. *There exists an $\varepsilon_0 > 0$ and constants $B, C > 0$ such that, for all $0 < \varepsilon < \varepsilon_0$* and *$0 \le n \le N$, the first $N+1$ eigenvalues $\lambda_0 > \ldots > \lambda_N$ of (4.13) satisfy:*

(a) *For $0 < \sigma_U < a^2/4$,*

$$\lambda_0 \in \left[\lambda_0^{*,\sigma_U} - C\varepsilon^{1/6}\mathrm{e}^{-B/\sqrt{\varepsilon}}, \lambda_0^{*,\sigma_L} + C\varepsilon^{1/6}\mathrm{e}^{-B/\sqrt{\varepsilon}}\right]$$

and

$$\lambda_n \in \left[\lambda_n^{*,\sigma_U} - C\varepsilon^{1/6}\mathrm{e}^{-B/\sqrt{\varepsilon}}, \lambda_n^{*,\sigma_L} + C\varepsilon^{1/6}\mathrm{e}^{-B/\sqrt{\varepsilon}}\right], \quad \textit{for all} \quad 1 \le n \le N.$$

(b) *For* $\sigma_L > a^2/4$,

$$\lambda_n \in \left[\lambda_{n+1}^{*,\sigma_U} - C\varepsilon^{1/6}\mathrm{e}^{-B/\sqrt{\varepsilon}}, \lambda_{n+1}^{*,\sigma_L} + C\varepsilon^{1/6}\mathrm{e}^{-B/\sqrt{\varepsilon}}\right], \quad \textit{for all} \quad 0 \le n \le N.$$

The proof of this theorem will be given in chapters 6, 7, and 8. This Theorem establishes the following facts:

1. There is an eigenvalue sequence $\lambda_1, \ldots, \lambda_N$ which is associated to the bifurcation of the DCM for $a > 0$. For buoyant species ($a < 0$), this eigenvalue sequence is associated to the bifurcation of the SL.
2. There is another eigenvalue λ_0 which is isolated in the sense that it is not part of the sequence with the DCMs and SLs. Instead it corresponds to a zero of a linear combination of the Airy function of the second kind and its derivative. This eigenvalue λ_0 is associated to the bifurcation of a BL for $a > 0$. We were not able to determine the structure of the other phytoplankton pattern, therefore we are not able to give any information concerning this isolated eigenvalue associated to $a < 0$.
3. The distance between successive eigenvalues is of $\mathcal{O}(\varepsilon^{1/3})$.
4. All first $N + 1$ eigenvalues of (4.13) are $\varepsilon^{1/3}$ close to λ^*, except for the special eigenvalue λ_0 if $\sigma_U < a^2/4$.
5. Up to exponentially small terms, the bounds on the eigenvalues are explicitly given in terms of zeros of the Airy functions Ai(x) and Bi(x) and their derivatives.
6. The width of the intervals that bound the eigenvalues λ_n of (4.13) is of the same order as the distance between successive eigenvalues, that is $\mathcal{O}(\varepsilon^{1/3})$.

In chapter 10 we will see that the eigenvalues established by Theorem 5.1 are quite sharp and agree very well with the bifurcations of the full (unscaled) model (4.1).

The analysis in chapters 6, 7, and 8 does not give any information on the structure of the associated eigenfunctions of (4.13). This is of particular interest to the nature of the of the patterns that are generated by (4.1) as λ_0 passes through zero. Also, Theorem 5.1 does not give any information about the transitional case $\sigma_L < a^2/4 < \sigma_U$.
Therefore, the analysis of (4.13) is completed by performing an asymptotic WKB

approximation in chapter 9. In [17] explicit formulas were derived for the eigenvalues and for the corresponding eigenfunctions for $a < 0$. In chapter 9 we will perform an asymptotic WKB approximation for $a < 0$, and we will use these explicit formulas to determine the profiles of the eigenfunctions for $a < 0$. Then we will explain what this means in biological terms.

The case $a > 0$, sinking species

- Case (a) of Theorem 5.1
  The profile of the eigenfunction ω_0, which corresponds to the largest eigenvalue λ_0, is of boundary layer type near the bottom.
  In terms of the phytoplankton concentration, this corresponds to a BL.

- Case(b) of Theorem 5.1
  The eigenfunction ω_0 has the shape of a spike around the point $x = x_{\mathrm{DCM}}$, where x_{DCM} is determined, to leading order in ε, by

  $$F(x_{\mathrm{DCM}}) = a^2/4$$

  In terms of the phytoplankton concentration, this profile corresponds to a DCM around x_{DCM}.

The case $a < 0$, buoyant species

- Case (a) of Theorem 5.1
  The eigenfunction ω_0 has a maximum around the point $x_{\max}$

  $$F(x_{\max}) = a^2/4 + \mathcal{O}(\varepsilon^{1/2}).$$

  The eigenfunction ω_0 has negative values in the beginning of the interval. For this reason, we were not able to determine the structure of the phytoplankton concentration in this case.

- Case (b) of Theorem 5.1
  The eigenfunction ω_0 is of boundary layer type near the surface. In terms of phytoplankton concentration, this corresponds to a SL.

The **transitional region** between the cases (a) and (b) in Theorem 5.1 is described to leading order in ε, by the equation $a^2/4 = F(1)$. Indeed, the leading order approximation of λ_0 is:

- $\lambda_0 = f(1) - \ell$ in the region $F(1) < a^2/4$.
  Sinking species: The eigenfunction ω_0 corresponds to a BL.
  Buoyant species: The eigenfunction ω_0 corresponds to the unknown structure.
- $\lambda_0 = f(0) - \ell - a^2/4$ in the region $F(1) > a^2/4$.
  Sinking species: The eigenfunction ω_0 corresponds to a DCM.
  Buoyant species: The eigenfunction ω_0 corresponds to a SL.

Recalling Lemma 5.1 we see that this transition occurs at a value of $a^2/4$ which is, always to leading order in ε, equal to

- σ_U when $0 < j_H \le j_H^{(1)}$,
- σ_L, when $j_H \ge j_H^{(2)}$,
- Between σ_U and σ_L, when $j_H^{(1)} < j_H < j_H^{(2)}$.

Lemma 5.1. *Let*

$$j_H^{(1)}(\kappa) = \frac{\mathrm{e}^{-\kappa} - 1 + \kappa}{\mathrm{e}^{\kappa} - 1 - \kappa} \quad \textit{and} \quad j_H^{(2)}(\kappa) = \frac{\mathrm{e}^{-\kappa}}{j_H^{(1)}(\kappa)},$$

so that $0 < j_H^{(1)}(\kappa) < j_H^{(2)}(\kappa) < 1$ *for all* $\kappa > 0$. *Also, define for all* $\kappa > 0$ *and* $j_H \in (j_H^{(1)}(\kappa), 1)$, *the point* $x_0 = x_0(\kappa, j_H) \in (0,1)$ *via* $F(x_0) = x_0 F'(x_0)$. *Then,*

$$\begin{aligned} \sigma_L(\kappa, j_H, \eta_H) &= \begin{cases} F'(0), & 0 < j_H \le j_H^{(2)}, \\ F(1), & j_H > j_H^{(2)}, \end{cases} \\ \sigma_U(\kappa, j_H, \eta_H) &= \begin{cases} F(1), & 0 < j_H \le j_H^{(1)}, \\ F'(x_0), & j_H^{(1)} < j_H < 1, \\ F'(0), & j_H \ge 1, \end{cases} \end{aligned} \tag{5.5}$$

and

$$\sigma_{L,U}(\kappa, j_H, \eta_H) = \nu \sigma_{L,U}(\kappa, j_H, 0), \quad \textit{with} \quad \nu = (1 + \eta_H)^{-1}. \tag{5.6}$$

Chapter 6

Eigenvalue bounds

In this chapter we make the first stepts towards the proof of Theorem 5.1. The results presented in this chapter apply to the case $a > 0$ and $a < 0$. To make the analysis easier we recast the eigenvalue problem (4.13) in a different form. First, we observe that the operator involved in this eigenvalue problem is self-adjoint only if $a = 0$. Applying the Liouville transformation

$$w(x) = e^{-ax/2\sqrt{\varepsilon}}\omega(x), \tag{6.1}$$

we obtain the self-adjoint problem

$$\begin{aligned} \varepsilon w_{xx} + (f(x) - \ell - (a^2/4))w &= \lambda w, \\ (\sqrt{\varepsilon}w_x - (a/2)w)(0) = (\sqrt{\varepsilon}w_x - (a/2)w)(1) &= 0. \end{aligned}$$

Recalling (5.1) and (5.4), we write this equation in the form

$$\mathcal{L}w = \mu w, \quad \text{with} \quad \mathcal{G}(w,0) = \mathcal{G}(w,1) = 0. \tag{6.2}$$

In this chapter we derive crude bounds for the eigenvalues of (6.2) in section 6.1, and tight bounds in section 6.2.

The operator $\mathcal{L}$, the scalar μ, and the linear functional $\mathcal{G}(\cdot, x)$ are defined by

$$\mathcal{L} = -\varepsilon\frac{d^2}{dx^2} + F(x), \quad \mu = \lambda^* - \lambda, \quad \mathcal{G}(w,x) = w(x) - \frac{2\sqrt{\varepsilon}}{a}w_x(x). \tag{6.3}$$

This is the desired form of the eigenvalue problem (4.13). We decompose $\mathcal{L}$ into a self-adjoint part for which (6.2) is solvable and a positive definite part. We use the following comparison principle to obtain the desired bounds.

Theorem 6.1. *Let the operators $\hat{\mathcal{A}}$ and $\mathcal{A}$ be self-adjoint, bounded below, and have compact inverses, and write their eigenvalues as $\hat{\mu}_0 \leq \hat{\mu}_1 \leq \ldots \leq \hat{\mu}_n \leq \ldots$ and $\mu_0 \leq \mu_1 \leq \ldots \leq \mu_n \leq \ldots$, respectively. If the difference $\mathcal{A} - \hat{\mathcal{A}}$ is positive semidefinite, then $\hat{\mu}_n \leq \mu_n$, for all $n \in \{0, 1, \ldots\}$.*

6.1 Crude bounds for the eigenvalues of $\mathcal{L}$

We derive crude bounds for the spectrum $\{\mu_n\}$ of $\mathcal{L}$ to demonstrate the method and to establish that $\mathcal{L}$ satisfies the boundedness condition of Theorem 6.1.

Lemma 6.1. *The eigenvalues μ_n satisfy the inequalities*

$$-a^2/4 \leq \mu_0 \leq F(1) - a^2/4 \quad \textit{and} \quad \varepsilon n^2\pi^2 \leq \mu_n \leq F(1) + \varepsilon^2 n^2\pi^2, \quad n \in \mathbf{N}. \tag{6.4}$$

Proof. Let $c \in R$. We start by decompositing $\mathcal{L}$ as

$$\mathcal{L} = \mathcal{L}^{0,c} + \mathcal{F}^{0,c}, \quad \text{where} \quad \mathcal{L}^{0,c} = -\varepsilon \frac{d^2}{dx^2} + c \quad \text{and} \quad \mathcal{F}^{0,c} = F(x) - c. \tag{6.5}$$

Then, we write $\left\{\mu_n^{0,c}\right\}$ for the set of eigenvalues of the problem

$$\mathcal{L}^{0,c} w^{0,c} = \mu^{0,c} w^{0,c}, \quad \text{with} \quad \mathcal{G}(w^{0,c}, 0) = \mathcal{G}(w^{0,c}, 1) = 0, \tag{6.6}$$

with the eigenvalues arranged so that $\mu_0^{0,c} \leq \mu_1^{0,c} \leq \ldots \leq \mu_n^{0,c} \leq \ldots$.

For $c = c_L = 0$, the operator $\mathcal{L}^{0,c_L}$ is self-adjoint, while $\mathcal{F}^{0,c_L} = F(x) \geq 0$ is a positive definite multiplicative operator. Thus, using Theorem 6.1, we obtain the following inequalities

$$\mu_n^{0,c_L} \leq \mu_n, \quad \text{for all} \quad n \in \mathbf{N} \cup \{0\}.$$

Next, for $c = c_U = F(1)$, the operator $\mathcal{F}^{0,c_U} = F(x) - F(1) \leq 0$ is negative definite, while $\mathcal{L}^{0,c_U}$ is self-adjoint. Hence, we write

$$\mathcal{L}^{0,c_U} = \mathcal{L} - \mathcal{F}^{0,c_U},$$

where $-\mathcal{F}^{0,c_U}$ is positive definite. The fact that the spectrum $\{\mu_n\}$ of $\mathcal{L}$ is bounded from below by (6.7) allows us to use Theorem 6.1 to bound each μ_n from above,

$$\mu_n \leq \mu_n^{0,c_U}, \quad \text{for all} \quad n \in \mathbf{N} \cup \{0\}.$$

Combining this bound and (6.7), we obtain

$$\mu_n^{0,c_L} \leq \mu_n \leq \mu_n^{0,c_U}, \quad \text{for all} \quad n \in \mathbf{N} \cup \{0\}. \tag{6.7}$$

Naturally, the eigenvalue problem (6.6) may be solved exactly to obtain

$$\mu_0^{0,c} = c - a^2/4 \quad \text{and} \quad \mu_n^{0,c} = c + \varepsilon n^2 \pi^2, \; n \in \mathbf{N} \tag{6.8}$$

Combining these formulas with (6.8), we obtain the inequalities (6.4). □

6.2 Tight bounds for the eigenvalues of $\mathcal{L}$

In Lemma 6.2, we bound the eigenvalues of μ_n by the eigenvalues $\mu_n^{1,\sigma}$ of a simpler problem. Then, in Lemma 6.3, we obtain strict, exponentially small bounds for $\mu_n^{1,\sigma}$.

Lemma 6.2. *Let $\sigma \in \{\sigma_L, \sigma_U\}$,with σ_L and σ_U as defined in (5.5), define the operator $\mathcal{L}^{1,\sigma} = \varepsilon \frac{d^2}{dx^2} + \sigma x$, and write $\mu_n^{1,\sigma}$ for the eigenvalues corresponding to the problem*

$$\mathcal{L}^{1,\sigma} w = \mu^{1,\sigma} w, \quad \textit{with} \quad \mathcal{G}(w,0) = \mathcal{G}(w,1) = 0. \tag{6.9}$$

Let $\left\{\mu_n^{1,\sigma}\right\}$ be arranged so that $\mu_0^{1,\sigma} \leq \mu_1^{1,\sigma} \leq \ldots \leq \mu_n^{1,\sigma} \leq \ldots$ Then,

$$\mu_n^{1,\sigma_L} \leq \mu_n \leq \mu_n^{1,\sigma_U}, \quad \textit{for all} \quad n \in \mathbf{N} \cup \{0\}. \tag{6.10}$$

Proof. First, we decompose $\mathcal{L}$ as

$$\mathcal{L} = \mathcal{L}^{1,\sigma} + \mathcal{F}^{1,\sigma}, \quad \text{where} \quad \mathcal{L}^{1,\sigma} = -\varepsilon \frac{d^2}{dx^2} + \sigma x, \; \mathcal{F}^{1,\sigma} = F(x) - \sigma x, \tag{6.11}$$

and $\sigma \in \{\sigma_L, \sigma_U\}$. We note here that $\mathcal{L}^{1,\sigma}$ is self-adjoint.

Next, $\mathcal{F}^{1,\sigma_L}$ is a positive definite multiplicative operator, since $F(x) \geq \sigma_L x$ (see (4.2)). Thus, $\mu_n^{1,\sigma_L} \leq \mu_n$, for all $n \in \mathbf{N} \cup \{0\}$, by Theorem 6.1. On the contrary, $\mathcal{F}^{1,\sigma_U}$ is negative definite, since $F(x) \leq \sigma_U x$. Therefore, we write

$$\mathcal{L}^{1,\sigma_U} = \mathcal{L} - \mathcal{F}^{1,\sigma_U},$$

where now $-\mathcal{F}^{1,\sigma_U}$ is positive definite. The fact that the spectrum $\{\mu_n\}$ is bounded from below by Lemma 6.1 allows us to use Theorem 6.1 to bound each μ_n from above, $\mu_n \leq \mu_n^{1,\sigma_U}$. Combining both bounds for each n, we obtain (6.11). □

The eigenvalue problem (6.10) is not exactly solvable, despite this fact we may calculate the eigenvalues up to terms exponentially small in ε. Recalling the definitions in chapter 5 and letting

$$\mu_0^{*,\sigma} = \lambda^* - \lambda_0^{*,\sigma} = -\sigma B_{0,\sigma} \quad \text{and} \quad \mu_n^{*,\sigma} = \lambda^* - \lambda_n^{*,\sigma} = \varepsilon^{1/3}\sigma^{2/3}|A'_{n,\sigma}| > 0 \tag{6.12}$$

for $n \geq 1$, we can state Lemma 6.3:

Lemma 6.3. *Let $N \in \mathbf{N}$ be fixed and $\bar{B} = 1 + B_{0,\sigma}$. We define*

$$\begin{aligned}
\delta_{0,\sigma} &= \varepsilon^{1/6}\sigma^{-1/6}\exp\left(-(2/3)[3(\bar{B}-B)^{3/2} - 2(B_{0,\sigma}-B)^{3/2} - (\bar{B}+B)^{3/2}]\sqrt{\sigma/\varepsilon}\right) \\
\delta_{n,\sigma} &= \varepsilon^{1/6}\exp\left(-(4/3)\sqrt{\sigma/\varepsilon} + 2|A_{n+1}|(\sigma/\varepsilon)^{3/2}\right), \quad \textit{for all} \quad 1 \leq n \leq N+1,
\end{aligned}$$

and for all $0 < B < B_{0,\sigma}$ for which the exponent in the expression for $\delta_{0,\sigma}$ is negative. Then, for each such B there is an $\varepsilon_0 > 0$ and positive constants $C_0, \ldots, C_{N+1}$, such that for all $0 < \varepsilon < \varepsilon_0$ and $0 \leq n \leq N$, the first $N+1$ eigenvalues $\mu_0^{1,\sigma}, \ldots, \mu_N^{1,\sigma}$ corresponding to (3.10) satisfy:

$$\begin{aligned}
&(a) \qquad \text{For} \quad 0 < \sigma < a^2/4, |\mu_0^{1,\sigma} - \mu_0^{*,\sigma}| < C_0\delta_{0,\sigma} \quad \textit{and} \quad |\mu_n^{1,\sigma} - \mu_n^{*,\sigma}| < C_n\delta_{n,\sigma}. \\
&(b) \qquad \text{For} \quad \sigma > a^2/4, |\mu_n^{1,\sigma} - \mu_{n+1}^{*,\sigma}| < C_{n+1}\delta_{n+1,\sigma}.
\end{aligned}$$

Part (a) is valid for all $1 \leq n \leq N$, and part (b) is valid for all $0 \leq n \leq N$.

The proof of this Lemma is given in chapter 7. The fact that these are indeed the $N + 1$ first eigenvalues corresponding to (6.10) is proved in chapter 7.

Theorem 5.1 follows by combining the three Lemmas in this chapter and using the definitions (5.4) and (6.13).

Chapter 7

The eigenvalues $\mu_0^{1,\sigma}, \ldots, \mu_N^{1,\sigma}$

In this section, we derive the bounds on $\mu_0^{1,\sigma}, \ldots, \mu_N^{1,\sigma}$ of Lemma 6.3. In section 7.1, we reduce the eigenvalue problem (6.10) to the algebraic one by formulating an Evans-type function $\mathcal{D}$ and identifying its roots. Then in section 7.2, we rewrite $\mathcal{D}$ in a different form, using two other functions $\mathcal{A}$ and $\mathcal{B}$ for the expression of $\mathcal{D}$. These two functions are easier to analyse. Finally, in the last section, we identify the roots of $\mathcal{D}$ by identifying the relevant roots of $\mathcal{A}$ and $\mathcal{B}$. All the results in this chapter are valid for $a > 0$ and $a < 0$.

7.1 Reformulation of the eigenvalue problem

First, we derive an algebraic equation whose solutions correspond to the eigenvalues of (6.10). We start by rescaling the parameter a, the small parameter ε, the eigenvalue $\mu_{1,\sigma}$, and the independent variable x via

$$\beta = \frac{a}{2\sqrt{\sigma}}, \quad 0 < \gamma \equiv \left(\frac{\varepsilon}{\sigma}\right)^{1/3} \ll 1, \quad \bar{\chi} = -\frac{\mu^{1,\sigma}}{\gamma\sigma}, \quad x = \gamma\left(\chi - \bar{\chi}\right), \tag{7.1}$$

and we note that the inequality $0 < \sigma < a^2/4$ becomes $\beta > 1$ if $a > 0$, and $\beta < 1$ if $a < 0$. The inequality $\sigma > a^2/4$ becomes $0 < \beta < 1$ if $a > 0$, and $-1 < \beta < 0$ if $a < 0$. Then, we define the linear functional

$$\Gamma(w, \bar{\chi}) = w(\bar{\chi}) - \frac{\sqrt{\gamma}}{\beta} w'(\bar{\chi}), \quad \text{for all differentiable functions } w, \tag{7.2}$$

and we remark that, for w equal to Ai and Bi, this definition agrees with the one given in (5.3).
Further introducing the Wronskian

$$\mathcal{D}(\bar{\chi}) = \Gamma(\mathrm{Ai}, \bar{\chi})\Gamma(\mathrm{Bi}, \gamma^{-1} + \bar{\chi}) - \Gamma(\mathrm{Ai}, \gamma^{-1} + \bar{\chi})\Gamma(\mathrm{Bi}, \bar{\chi}) \tag{7.3}$$

we can prove the following lemma.

Lemma 7.1. *The eigenvalue problem (6.10) has $\mu^{1,\sigma}$ as an eigenvalue if and only if $\mathcal{D}(\bar{\chi}) = 0$.*

Proof. Using (7.1) we rewrite problem (6.10) in the form

$$\begin{aligned} \frac{d^2 w}{d\chi^2} &= \chi w, \quad \chi \in [\bar{\chi}, \gamma^{-1} + \bar{\chi}] \\ \Gamma(w, \bar{\chi}) = \Gamma(w, \gamma^{-1} + \bar{\chi}) &= 0. \end{aligned} \tag{7.4}$$

This is an Airy equation and thus has the general solution

$$w(\chi) = D_A \mathrm{Ai}(\chi) + D_B \mathrm{Bi}(\chi). \tag{7.5}$$

The boundary condition becomes

$$\begin{aligned} \Gamma(w, \bar{\chi}) &= D_A \Gamma(\mathrm{Ai}, \bar{\chi}) + D_B \Gamma(\mathrm{Bi}, \bar{\chi}) = 0, \\ \Gamma(w, \gamma^{-1} + \bar{\chi}) &= D_A \Gamma(\mathrm{Ai}, \gamma^{-1} + \bar{\chi}) + D_B \Gamma(\mathrm{Bi}, \gamma^{-1} + \bar{\chi}) = 0. \end{aligned} \tag{7.6}$$

The sufficient and necessary condition for the existence of nontrivial solutions to this system is that its determinant, which is the Wronskian $\mathcal{D}$ given in (7.3), vanishes, and the lemma is proved. □

Thus we see that the values of $\bar{\chi}$ that corresponds to the eigenvalues $\mu^{1,\sigma}$ are zeros of $\mathcal{D}$.

7.2 Product decomposition of the function $\mathcal{D}$

To identify the roots of $\mathcal{D}$, we rewrite $\mathcal{D}$ in the form

$$\mathcal{D}(\bar{\chi}) = \Gamma(\mathrm{Bi}, \gamma^{-1} + \bar{\chi})\mathcal{A}(\bar{\chi}) = \Gamma(\mathrm{Ai}, \bar{\chi})\mathcal{B}(\bar{\chi}), \tag{7.7}$$

where we have defined the functions

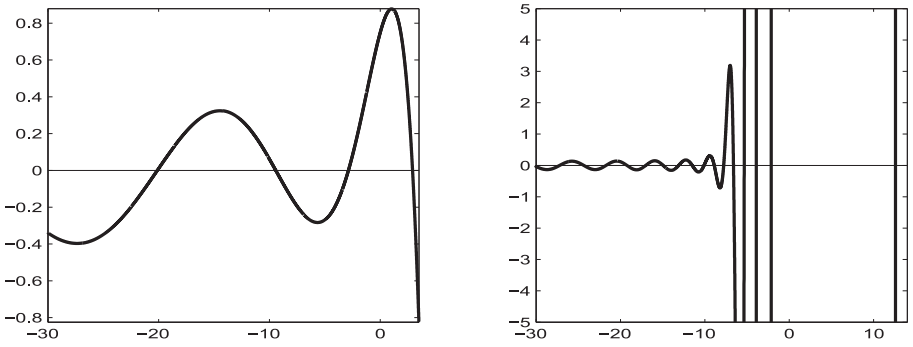

Figure 7.1: The function $\mathcal{D}(\bar{\chi})$ for $a = 3$, $\sigma = 1$, and $\varepsilon = 0.1$ (left panel), $\varepsilon = 0.001$ (right panel).

$$\mathcal{A}(\bar{\chi}) = \Gamma(\mathrm{Ai}, \bar{\chi}) - \frac{\Gamma(\mathrm{Ai}, \gamma^{-1} + \bar{\chi})}{\Gamma(\mathrm{Bi}, \gamma^{-1} + \bar{\chi})}\Gamma(\mathrm{Bi}, \bar{\chi}), \tag{7.8}$$

$$\mathcal{B}(\bar{\chi}) = \Gamma(\mathrm{Bi}, \gamma^{-1} + \bar{\chi}) - \frac{\Gamma(\mathrm{Bi}, \bar{\chi})}{\Gamma(\mathrm{Ai}, \bar{\chi})}\Gamma(\mathrm{Ai}, \gamma^{-1} + \bar{\chi}). \tag{7.9}$$

Here, $\mathcal{A}$ is well-defined for all $\bar{\chi}$ such that $\Gamma(\mathrm{Bi}, \gamma^{-1} + \bar{\chi}) \neq 0$, while $\mathcal{B}$ is well-defined for all $\bar{\chi}$ such that $\Gamma(\mathrm{Ai}, \bar{\chi}) \neq 0$. Equation (7.7) implies that the roots of $\mathcal{A}$ and $\mathcal{B}$ are also roots of $\mathcal{D}$.

In the next section, we will prove that the first few zeros of $\mathcal{D}$ are all $\mathcal{O}(1)$, in the case $0 < \beta < 1$. The zeros are both $\mathcal{O}(1)$ and $\mathcal{O}(\gamma^{-1})$ in the case $\beta > 1$. We will also establish that the $\mathcal{O}(1)$ roots of $\mathcal{D}$ coincide with roots of the function $\mathcal{A}$ and the $\mathcal{O}(\gamma^{-1})$ ones with the function $\mathcal{B}$. To prove this, we first characterise the behaviours of $\mathcal{A}$ and $\mathcal{B}$ for $\mathcal{O}(1)$ and $\mathcal{O}(\gamma^{-1})$ values of $\bar{\chi}$, respectively, in the next two lemmas. We write $E(x) = \exp(-(2/3)x^{3/2})$ and

$$||w||_{[X_L, X_R]} = \max_{\bar{\chi} \in [X_L, X_R]} |w(\bar{\chi})| + \max_{\bar{\chi} \in [X_L, X_R]} |w'(\bar{\chi})|. \tag{7.10}$$

Lemma 7.2. *Let X be fixed. Then, there is a $\gamma_0 > 0$ and a constant $c_A > 0$ such that*

$$||\mathcal{A}(\bar{\chi}) - \Gamma(\mathrm{Ai}, \bar{\chi})||_{[X,0]} < c_A \gamma^{-1/2} E(\gamma^{-1}(2 + 3X\gamma)^{2/3}), \tag{7.11}$$

for all $0 < \gamma < \gamma_0$.

For the next lemma we switch to the independent variable $\bar{\psi} = \gamma\bar{\chi}$ to make the calculations easier. We analyse the behaviour of $\mathcal{B}(\gamma^{-1}\bar{\psi})$ for $\mathcal{O}(1)$ values of $\bar{\psi}$ (equivalently, for $\mathcal{O}(\gamma^{-1})$ values of $\bar{\chi}$) as $\gamma \downarrow 0$.

Lemma 7.3. *Let $0 < \Psi_L < \Psi_R$ be fixed. Then, there is a γ_0 and a constant $c_B > 0$ such that, for all $0 < \gamma < \gamma_0$,*

$$||E(\gamma^{-1}(1+\bar{\psi}))[\mathcal{B}(\gamma^{-1}\bar{\psi}) - \Gamma(\mathrm{Bi}, \gamma^{-1}(1+\bar{\psi}))]||_{[\Psi_L,\Psi_R]} < c_B\gamma^{-1/4}\left[\frac{E(\gamma^{-1}(1+\Psi_L))}{E(\gamma^{-1}\Psi_L)}\right]^2$$

The proofs of these two lemmas are given in Appendix B and C.

7.3 Zeros of the function $\mathcal{D}$

We use the above results and the following lemma to locate the roots of $\mathcal{D}$.

Lemma 7.4. *Let $N \in \mathbf{N}$ be fixed, $A'_{n,\sigma}$ and $B_{0,\sigma}$ be defined as in chapter 5, and B, $\delta_{0,\sigma}, \ldots, \delta_{N,\sigma}$ as in Lemma 6.3. Then for each admissible B, there is a $\gamma_0 > 0$ and positive constants $c_0, \ldots, c_n$ such that, for all $0 < \gamma < \gamma_0$, the function $\mathcal{D}(\bar{\chi})$ has roots $\bar{\chi}_0 > \bar{\chi}_1 > \ldots > \bar{\chi}_N$ which satisfy the following bounds:*

(a) For $\beta > 1$ (equivalently $0 < \sigma < a^2/4$),

$$|\bar{\chi}_0 - \gamma^{-1}B_{0,\sigma}| < c_0\gamma^{-1}\delta_{0,\sigma}, \quad |\bar{\chi_n} - A'_{n,\sigma}| < c_n\gamma^{-1}\delta_{n,\sigma}, \quad \textit{for all} \quad 1 \le n \le N.$$

(b) For $0 < \beta < 1$ (*equivalently $\sigma > a^2/4$*),

$$|\bar{\chi_n} - A'_{n+1,\sigma}| < c_n\gamma^{-1}\delta_{n+1,\sigma}, \quad \textit{for all} \quad 0 \le n \le N.$$

For buoyant species, in part (a) of Lemma 7.4 $\beta > 1$ is be replaced by $\beta < 1$ and in part (b), $0 < \beta < 1$ is replaced by $-1 < \beta < 0$. To prove this lemma we need the following result.

Lemma 7.5. *Let C, G, and H be real-valued, continuous functions. Let $\delta > 0$ and $z_0 \in [Z_L, Z_R] \subset \mathbf{R}$ be such that*

$$H(z_0) = 0, \quad \max_{[Z_L, Z_R]} H' = -H_0 < 0, \quad \max_{[Z_L, Z_R]} |C(G-H)| < \delta \quad \textit{and} \quad \min_{[Z_L, Z_R]} C = C_0 > 0.$$

If $\delta < C_0 H_0 \min(z_0 - Z_L, Z_R - z_0)$, then G has a zero z^* such that $|z^* - z_0| \leq \delta/(C_0 H_0)$.

Proof. Let $z_\ell = z_0 - \delta/(C_0 H_0)$ and $z_r = z_0 + \delta/(C_0 H_0)$. By assumption, $Z_L < z_\ell < z_0 < z_r < Z_R$, and thus

$$G(z_\ell) \geq \int_{z_0}^{z_\ell} H'(z)dz - \frac{\max_{[Z_L, Z_R]} |C(G-H)|}{\min_{[Z_L, Z_R]} C} > (z_0 - z_\ell)H_0 - \frac{\delta}{C_0} = 0,$$

where we write $G(z_\ell) = H(z_\ell) + G(z_\ell) - H(z_\ell)$. Similarly, we may prove that $G(z_r) < 0$ and the desired result follows. □

Proof. (Lemma 7.4.) First, we prove the existence of a root $\bar{\chi}_0$ satisfying the desired bound. We start by rescaling the independent variable through $\bar{\psi} = \gamma\bar{\chi}$. Then, it suffices to show that there is a root $\bar{\psi}_0$ of $\mathcal{D}(\gamma^{-1}\bar{\psi})$ satisfying the bound $|\bar{\psi}_0 - B_{0,\sigma}| < c_0\delta_0$, for some $c_0 > 0$. Equation (7.7) reads

$$D(\gamma^{-1}\bar{\psi}) = \Gamma(\mathrm{Ai}, \gamma^{-1}\bar{\psi})\mathcal{B}(\gamma^{-1}\bar{\psi}).$$

Here, $\Gamma(\mathrm{Ai}, \gamma^{-1}\bar{\psi})$ has no positive roots, by definition of Γ and because $\mathrm{Ai}(\gamma^{-1}\bar{\psi}) > 0$ and $\mathrm{Ai}'(\gamma^{-1}\bar{\psi}) < 0$, for all $\bar{\psi} > 0$. Thus, $\bar{\chi}_0$ must be a root of $\mathcal{B}$. Its existence and the bound on it follow from Lemmas 7.3 and 7.5. Indeed, let

$$z_0 = B_{0,\sigma}, \quad Z_L = B_{0,\sigma} - B, \quad Z_R = B_{0,\sigma} + B,$$
$$C = E, \quad G = \mathcal{B}, \quad H = \Gamma(\mathrm{Bi}, \cdot).$$

Lemma 7.3 provides a bound δ on $||C(G-H)||_{[Z_L, Z_R]}$. Also, using the expressions for the Airy functions in Appendix A, we may calculate

$$C_0 = \min_{[Z_L, Z_R]} E(\gamma^{-1}(1+\bar{\psi})) = E(\gamma^{-1}(1+Z_r)),$$

$$-H_0 = \max_{[Z_L, Z_R]} \Gamma(\mathrm{Bi}', \gamma^{-1}(1+\bar{\psi})) < c\gamma^{-1/4}[E(\gamma^{-1}(1+Z_L))]^{-1}.$$

Now, δ satisfies the condition $\delta < C_0 H_0 B$ of Lemma 7.5 for all γ small enough. Thus we may apply Lemma 7.5 to obtain the desired bound on $\bar{\chi}_0$. That is,

$$\delta = c_B \gamma^{1/4} \left[\frac{E(\gamma^{-1}(1+\psi))}{E(\gamma^{-1}\psi)} \right]^2 .$$

Next we show that $\mathcal{A}$ has the remaining roots $\bar{\chi}_1, \ldots, \bar{\chi}_N$. We fix $A_{N+1} < X < A_N$ and let $I_1, \ldots, I_N$ be disjoint intervals around $A_1, \ldots, A_N$, respectively. Lemma 7.2 states that $\mathcal{A}(\bar{\chi})$ and $\Gamma(\mathrm{Ai}, \bar{\chi})$ are exponentially close in the W_∞^1-norm over $[X, 0]$. Thus, for all $0 < \gamma < \gamma_0$ (with γ_0 small enough), $\mathcal{A}$ has N distinct roots $\bar{\chi}_1 \in I_1, \ldots, \bar{\chi}_N \in I_N$ in $[X, 0]$ by Lemma A.2. Since $\Gamma(\mathrm{Bi}, \gamma^{-1} + \bar{\chi})$ can be bounded away from zero over $[X, 0]$ using the expressions for the Airy functions in Appendix A, we conclude that $\mathcal{D}$ has N distinct roots $\bar{\chi}_1, \ldots, \bar{\chi}_N$ in $[X, 0]$.

(b) The argument used in part (a)- where $\beta > 1$ - to establish the bounds on the $\mathcal{O}(1)$ roots of $\mathcal{A}$ does not depend on the sign of $\beta - 1$. Therefore, it applies also to this case - where $0 < \beta < 1$ - , though in an interval $[X, 0]$, with $A_{N+2} < X < A_{N+1}$, yielding $N + 1$ roots which we label $\bar{\chi}_0, \ldots, \bar{\chi}_N$.

On the other hand, $B_{0,\sigma} < 0$ for $0 < \beta < 1$, because of the estimate on $B_{0,\sigma}$ in Lemma A.2. As a result, the argument used to identify that root does not apply anymore, since $B_{0,\sigma} < 0$ and thus Lemma 7.3 may not be applied to provide the bound δ needed in Lemma 7.5. In fact, were this roots to persist and remain close to $\gamma - 1 B_{0,\sigma}$ as in case (a), it would become large and negative by the estimate in Lemma A.2 and thus smaller than the roots $\bar{\chi}_0, \ldots, \bar{\chi}_N$ obtained above. Thus it could never be the leading value in this parameter regime.

□

By rescaling back to the original parameters we obtain the bounds on the eigenvalues $\mu_0^{1,\sigma}, \ldots, \mu_N^{1,\sigma}$ in Lemma 3.3.

Chapter 8

The eigenfunctions $w_0^{1,\sigma}, \ldots, w_N^{1,\sigma}$

In this chapter we derive formulas for the eigenfunctions $w_0^{1,\sigma}, \ldots, w_N^{1,\sigma}$ associated with the eigenvalues $\mu_0^{1,\sigma}, \ldots, \mu_N^{1,\sigma}$, respectively. We will show that each eigenfunction $w_n^{1,\sigma}$ has n zeros in the interval $[\bar{\chi}_n, \gamma^{-1} + \bar{\chi}_n]$. This will be proved in the following lemma. In this way, we can show that these eigenvalues are the largest ones.

Lemma 8.1. *Let $N \in \mathbf{N}$. Then, there is a $\gamma_0 > 0$ such that, for all $0 < \gamma < \gamma_0$ and for all $n = 0, 1, \ldots, N$, the eigenfunction $w_n^{1,\sigma}$ corresponding to the eigenvalue $\mu_n^{1,\sigma}$ has exactly n zeros in the interval $[\bar{\chi}_n, \gamma^{-1} + \bar{\chi}_n]$.*

This lemma will be proved in section 8.1 for the cases $\beta > 1$ and $\beta < -1$. In section 8.2 it will be proved for the cases $0 < \beta < 1$ and $-1 < \beta < 0$. For each case we determine the function ω_0 and study the profiles associated with this function. The cases $\beta > 1$ and $0 < \beta < 1$ corresponding to the case $a > 0$, sinking species, were found in [17]. The cases $\beta < -1$ and $-1 < \beta < 0$ corresponding to $a < 0$, the buoyant species, were found in this thesis.

The profiles in section 8.1

- $\beta > 1$: De eigenfunction ω_0 has a boundary layer at $x = 1$.
- $\beta < -1$: De eigenfunction ω_0 has a maximum at $x_{\max} = (-\beta)^{4/3} - \beta^2 + 1$.

The profiles in section 8.2

- $0 < \beta < 1$: De eigenfunction ω_0 has a spike around the point

$$|x_\beta - (\beta^2 + |A_1|\gamma)| < c\gamma^2, \quad \text{for some} \quad c > 0.$$

- $-1 < \beta < 0$: De eigenfunction ω_0 has a boundary layer at $x = 0$.

We start by fixing $\bar{\chi}$ to be $\bar{\chi}_n$, for some $n = 1, \ldots, N$. The corresponding **eigenvalue** is

$$\mu_n^{1,\sigma} = -\gamma\sigma\bar{\chi}_n,$$

while the corresponding **eigenfunction** w_n is given by (7.5),

$$w_n^{1,\sigma}(\chi) = D_A \mathrm{Ai}(\chi) + D_B \mathrm{Bi}(\chi), \quad \text{where} \quad \chi \in \left[\bar{\chi}_n, \gamma^{-1} + \bar{\chi}_n\right] \tag{8.1}$$

Here the coefficients D_A and D_A satisfy (7.6),

$$D_A\Gamma_{L,n}(\mathrm{Ai}) + D_B\Gamma_{L,n}(\mathrm{Bi}) = D_A\Gamma_{R,n}(\mathrm{Ai}) + D_B\Gamma_{R,n}(\mathrm{Bi}) = 0,$$

where

$$\Gamma_{L,n}(\cdot) = \Gamma(\cdot, \bar{\chi}_n), \quad \text{and} \quad \Gamma_{R,n}(\cdot) = \Gamma(\cdot, \gamma^{-1} + \bar{\chi}_n).$$

8.1 The cases $\beta > 1$ and $\beta < -1$

In this section, we select D_A and D_B so that (8.1) becomes

$$w_n^{1,\sigma}(\chi) = D_n \mathrm{Bi}(\chi) - \mathrm{Ai}(\chi), \quad \text{with} \quad D_n = \frac{\Gamma_{L,n}(\mathrm{Ai})}{\Gamma_{L,n}(\mathrm{Bi})} \tag{8.2}$$

We use this formula to prove Lemma 8.1 for $\beta > 1$ and $\beta < 1$. In section 8.1.1 we prove that $w_0^{1,\sigma}$ has no zeros in $[\bar{\chi}_0, \gamma^{-1} + \bar{\chi}_0]$, then we evaluate D_0 and the eigenfuntion $\omega_0(x)$. In section 8.1.2 we study $\omega_0(x)$ for each case separately and determine the profile for each case. In section 8.1.3 we show that the eigenfunction $w_n^{1,\sigma}$ has exactly n zeros in $[\bar{\chi}_n, 0]$ and we evaluate D_n.

8.1.1 The eigenfunction $w_0^{1,\sigma}$

First, we show that $w_0^{1,\sigma}$ has no zeros in the interval $[\bar{\chi}_0, \gamma^{-1} + \bar{\chi}_0]$. We need the following expression

$$D_0 = \left(\frac{\Delta_1^2}{2} + \bar{C}_0(\gamma)\right) \exp\left(-4\left(\frac{(\beta^2-1)^{3/2}}{3\gamma^{3/2}} + \sqrt{1 - \frac{1}{\beta^2}}\right)\right).$$

Here, $\Delta_1^2 = (\beta + \sqrt{\beta^2 - 1})/(\beta - \sqrt{\beta^2 - 1})$ and $|\bar{C}_0(\gamma)| < c_0\gamma^{3/2}$, for some $c_0 > 0$. Thus also, $D_0 > 0$.

The eigenfunction $w_0^{1,\sigma}$ has no zeros in the interval $[\bar{\chi}_0, \gamma^{-1} + \bar{\chi}_0]$.

First, we prove that $(w_0^{1,\sigma})' > 0$ everywhere on the interval. Then we show that $w_0^{1,\sigma}(\bar{\chi}_0) > 0$ if $\beta > 1$ (sinking species), and $w_0^{1,\sigma}(\bar{\chi}_0) < 0$ if $\beta < -1$ (buoyant species). For $n = 0$, (8.2) yields $(w_0^{1,\sigma})'(\chi) = D_0\mathrm{Bi}'(\chi) - \mathrm{Ai}'(\chi)$, and Lemma 7.4 shows that $[\bar{\chi}_0, \gamma^{-1}\bar{\chi}_0] \subset \mathbf{R}_+$. Hence, $\mathrm{Bi}'(\chi) > 0$ and $\mathrm{Ai}'(\chi) < 0$ for all χ in this interval. Since $D_0 > 0$ we can conclude that $(w_0^{1,\sigma})' > 0$. Next, we determine the sign of $w_0^{1,\sigma}(\bar{\chi}_0)$. The definition of $\Gamma_{L,0}$ yields

$$\mathrm{Ai}(\bar{\chi}_0) = \Gamma_{L,0}(\mathrm{Ai}) + \beta^{-1}\sqrt{\gamma}\mathrm{Ai}'(\bar{\chi}_0).$$
$$\mathrm{Bi}(\bar{\chi}_0) = \Gamma_{L,0}(\mathrm{Bi}) + \beta^{-1}\sqrt{\gamma}\mathrm{Bi}'(\bar{\chi}_0).$$

Substituting these expressions in the function $w_0^{1,\sigma}(\bar{\chi}_0)$ in (8.2), we find that

$$w_0^{1,\sigma}(\bar{\chi}_0) = \beta^{-1}\sqrt{\gamma}[D_0\mathrm{Bi}'(\bar{\chi}_0) - \mathrm{Ai}'(\bar{\chi}_0)].$$

Thus we see that $w_0^{1,\sigma}(\bar{\chi}_0) > 0$ if $\beta > 1$ and $w_0^{1,\sigma}(\bar{\chi}_0) < 0$ if $\beta < -1$, by our remarks on the signs of Bi', Ai' and D_0. In the same way we find that $w_0^{1,\sigma}(\gamma^{-1} + \bar{\chi}_0) > 0$ if $\beta > 1$, and $w_0^{1,\sigma}(\gamma^{-1} + \bar{\chi}_0) < 0$ if $\beta < -1$. This completes the proof.

The estimation D_0.

From (8.2) and the formulas for $\mathrm{Ai}(z)$, $\mathrm{Bi}(z)$ in Appendix A, we find that

$$\frac{\Gamma(\mathrm{Ai}, z)}{\Gamma(\mathrm{Bi}, z)} = \frac{\mathrm{Ai}(z) - \beta^{-1}\sqrt{\gamma}\mathrm{Ai}'(z)}{\mathrm{Bi}(z) - \beta^{-1}\sqrt{\gamma}\mathrm{Bi}'(z)} = \frac{1}{2}\frac{\beta + \gamma^{1/2}z^{1/2}}{\beta - \gamma^{1/2}z^{1/2}}\exp\left(-(4/3)z^{3/2}\right).$$

Here we have for $n = 0$

$$D_0 = \frac{\Gamma_{L,0}(\mathrm{Ai})}{\Gamma_{L,0}(\mathrm{Bi})} = \frac{1}{2}\frac{\beta + \gamma^{1/2}\bar{\chi}_0^{1/2}}{\beta - \gamma^{1/2}\bar{\chi}_0^{1/2}}\exp\left(-(4/3)\bar{\chi}_0^{3/2}\right).$$

Using the estimates of Lemma 7.4. for $\bar{\chi}_0$ and A.2 for $B_{0,\sigma}$ we find that

$$\bar{\chi}_0 = \gamma^{-1}B_{0,\sigma} = \gamma^{-1}\left(\beta^2 - 1 + 2\beta^{-1}\gamma^{3/2}\right).$$

Using Taylor's theorem we find that

$$\begin{aligned} \bar{\chi}_0^{1/2} &= \gamma^{-1/2}(\beta^2-1)^{1/2} + \gamma\beta^{-1}(\beta^2-1)^{-1/2} \\ \bar{\chi}_0^{3/2} &= \gamma^{-3/2}(\beta^2-1)^{3/2} + 3\beta^{-1}(\beta^2-1)^{1/2}. \end{aligned}$$

Thus

$$D_0 = \frac{1}{2}\frac{\beta+\sqrt{\beta^2-1}+c(\beta)\gamma^{3/2}}{\beta-\sqrt{\beta^2-1}-c(\beta)\gamma^{3/2}}\exp\left(-4\left(\frac{(\beta^2-1)^{3/2}}{3\gamma^{3/2}}+\beta^{-1}\sqrt{\beta^2-1}\right)\right)$$

with $c(\beta) = \beta^{-1}(\beta^2-1)^{-1/2}$.

We rewrite this expression for D_0 in a simpler form. Let

$$G_\beta(\gamma) = \frac{\beta+\sqrt{\beta^2-1}+c(\beta)\gamma^{3/2}}{\beta-\sqrt{\beta^2-1}-c(\beta)\gamma^{3/2}} \quad \text{and} \quad g(\gamma) = \frac{1}{\beta-\sqrt{\beta^2-1}-c(\beta)\gamma^{3/2}}.$$

Then,

$$\begin{aligned} G_\beta(\gamma) &= \left(\beta+\sqrt{\beta^2-1}+c(\beta)\gamma^{3/2}\right)\left(\frac{1}{\beta-\sqrt{\beta^2-1}}+\frac{c(\beta)}{(\beta-\sqrt{\beta^2-1})^2}\gamma^{3/2}\right) \\ &= \frac{\beta+\sqrt{\beta^2-1}}{\beta-\sqrt{\beta^2-1}} + c_1(\beta)\gamma^{3/2} + c_2(\beta)\gamma^3, \end{aligned}$$

where $c_1(\beta) = \frac{2\beta c(\beta)}{\beta-\sqrt{\beta^2-1}}$ and $c_2(\beta) = \frac{c(\beta)^2}{(\beta-\sqrt{\beta^2-1})^2}$.

We write $(1/2)G_\beta(\gamma) = (1/2)\Delta_1^2 + \bar{C}_0(\gamma)$ where $\Delta_1^2 = \frac{\beta+\sqrt{\beta^2-1}}{\beta-\sqrt{\beta^2-1}}$ and $\bar{C}_0(\gamma) = (1/2)\left(c_1(\beta)\gamma^{3/2} + c_2(\beta)\gamma^3\right)$.

From this it follows that $|\bar{C}_0(\gamma)| < c_0\gamma^{3/2}$. This gives the desired result.

The eigenfunction ω_0.

Equations (6.1) and (7.1) yield

$$\omega_0(x) = \exp\left(\frac{\beta}{\gamma^{3/2}}x\right)[D_0\mathrm{Bi}(\gamma^{-1}x+\bar{\chi}_0) - \mathrm{Ai}(\gamma^{-1}x+\bar{\chi}_0)], \quad x \in [0,1].$$

We can now find $\omega_0(x)$ using the estimation of Lemma 5.4 for $\bar{\chi}_0$ and the expressions $\mathrm{Ai}(z)$ and $\mathrm{Bi}(z)$

$$\omega_0(x) = C_I(x+\beta^2-1)^{-1/4}\exp\left(\frac{\beta}{\gamma^{3/2}}x\right)\sinh(\theta_1(x)), \quad x\in[0,1], \tag{8.3}$$

where $C_I = (\pi^{-1/2})\gamma^{1/4}\exp(-\tilde{c}\gamma^{-3/2}+\tilde{c}_0)$, $|C_I| < c_I\gamma^{1/4}$ for some $c_I > 0$, and

$$\theta_1(x) = \frac{2}{3\gamma^{3/2}}\left[(x+\beta^2-1)^{3/2}-(\beta^2-1)^{3/2}\right] + \frac{2}{\beta}\left[(x+\beta^2-1)^{1/2}-(\beta^2-1)^{1/2}\right] + \log\Delta_1.$$

We show how we have derived ω_0, in four steps. Here we have $\gamma^{-1}x+\bar{\chi}_0 = \gamma^{-1}(x+\beta^2-1+2\beta^{-1}\gamma^{3/2})$. Thus

$$\begin{aligned}(\gamma^{-1}x+\bar{\chi}_0)^{-1/4} &= \gamma^{1/4}(x+\beta^2-1)^{-1/4} - \gamma^{7/4}\frac{1}{2}\beta^{-1}(x+\beta^2-1)^{-5/4}\\ (\gamma^{-1}x+\bar{\chi}_0)^{3/2} &= \gamma^{-3/2}(x+\beta^2-1)^{3/2} + 3\beta^{-1}(x+\beta^2-1)^{1/2}\end{aligned}$$

Step 1

$$\mathrm{Bi}(\gamma^{-1}x+\bar{\chi}_0) = \pi^{-1/2}(x+\beta^2-1)^{-1/4}\exp\left(\frac{2(x+\beta^2-1)^{3/2}}{3\gamma^{3/2}} + 2\beta^{-1}(x+\beta^2-1)^{1/2}\right).$$

Step 2

$$D_0\mathrm{Bi}(\gamma^{-1}x+\bar{\chi}_0) = \left(\frac{\Delta_1^2}{2}+\bar{C}_0(\gamma)\right)\left(\pi^{-1/2}\gamma^{1/4}(x+\beta^2-1)^{-1/4}\right)\exp\left(\varphi(x)\right).$$

we neglect the higher order term $\bar{C}_0$ and write

$$D_0\mathrm{Bi}(\gamma^{-1}x+\bar{\chi}_0) = \left(\pi^{-1/2}\gamma^{1/4}(x+\beta^2-1)^{-1/4}\right)\exp\left(\varphi(x)\right),$$

with

$$\varphi(x) = \frac{2}{3\gamma^{3/2}}\left[(x+\beta^2-1)^{3/2}-2(\beta^2-1)^{3/2}\right] + \frac{2}{\beta}\left[(x+\beta^2-1)^{1/2}-2\sqrt{\beta^2-1}\right] + \log\Delta_1^2.$$

Step 3

$$\mathrm{Ai}(\gamma^{-1}x+\bar{\chi}_0) = \frac{1}{2}\pi^{-1/2}\gamma^{1/4}(x+\beta^2-1)^{-1/4}\exp\left(\frac{-2(x+\beta^2-1)^{3/2}}{3\gamma^{3/2}} - \frac{2}{\beta}(x+\beta^2-1)^{1/2}\right).$$

Step 4
To make calculations easier we write

$$\begin{aligned}\varphi_0(x) &= \frac{2}{3\gamma^{3/2}}(x+\beta^2-1)^{3/2}+\frac{2}{\beta}(x+\beta^2-1)^{1/2}.\\ \varphi_1 &= -\frac{4}{3\gamma^{3/2}}(\beta^2-1)^{3/2}-\frac{4}{\beta}\sqrt{\beta^2-1}+\log\Delta_1^2.\end{aligned}$$

and $\varphi(x)=\varphi_0(x)+\varphi_1$. Then,

$$\begin{aligned}D_0\mathrm{Bi}(\gamma^{-1}x+\bar{\chi}_0)-\mathrm{Ai}(\gamma^{-1}x+\bar{\chi}_0) &= (1/2)\pi^{-1/2}\gamma^{1/4}\hat{\beta}^{-1/4}\left(e^{\varphi_0+\varphi_1}-e^{-\varphi_0}\right)\\ &= \pi^{-1/2}\gamma^{1/4}(x+\beta^2-1)^{-1/4}e^{(1/2)\varphi_1}\sinh(\theta_1(x)),\end{aligned}$$

where $\theta_1(x)=(1/2)\left(e^{\varphi_0+(1/2)\varphi_1}-e^{-(\varphi_0+(1/2)\varphi_1)}\right)$. Thus

$$\omega_0(x)=C_I(x+\beta^2-1)^{-1/4}\exp\left(\frac{\beta}{\gamma^{3/2}}x\right)\sinh(\theta_1(x)).$$

where

$$C_I=(\pi^{-1/2})\gamma^{1/4}\exp\left(-\frac{2}{3\gamma^{3/2}}(\beta^2-1)^{3/2}-\frac{2}{\beta}\sqrt{\beta^2-1}+\log\Delta_1\right).$$

8.1.2 The profiles

The profile for $\beta > 1$, sinking species

To leading order we can write

$$\omega_0(x)=b_1\exp\left(\frac{\beta}{\gamma^{3/2}}x\right)\sinh\left(\frac{2}{3\gamma^{3/2}}b_2\right),$$

where $b1, b2 > 0$ are constants. If $x \to 1$, $\exp\left(\frac{\beta}{\gamma^{3/2}}x\right) \to \infty$, and $\sinh\left(\frac{1}{\gamma^{3/2}}(2/3)c_2\right) \to \infty$ because γ is very small. Hence $\omega_0(x) \to \infty$. Thus $\omega_0(x)$ corresponds to a boundary layer at $x = 1$ (Figure 8.1), which is of width $\mathcal{O}(\varepsilon^{3/2})$.

The profile for $\beta < -1$, buoyant species

The function $\omega_0(x)$ has a maximum at

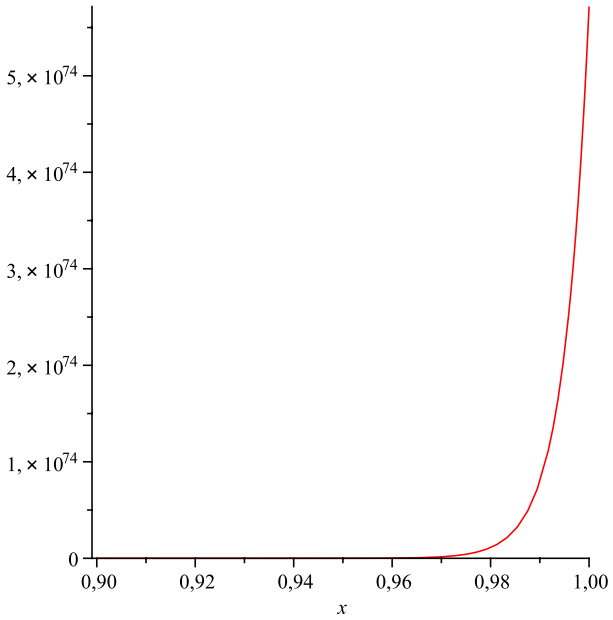

Figure 8.1: **Sinking species** The function $w_0(x)$ corresponds to a boundary layer at $x = 1$. Here, $\beta = 1.1$ and $\gamma = 0.05$.

$$x_{\max} = (-\beta)^{4/3} - \beta^2 + 1. \tag{8.4}$$

The function takes on negative values at the beginning of the interval, see Figure 8.2.

8.1.3 The eigenfunctions $w_1^{1,\sigma}, \ldots, w_N^{1,\sigma}$

The eigenfunction $w_n^{1,\sigma}$ is given by (8.2), where the estimation D_n is

$$D_n = \left(\frac{\Delta_2^2}{2} + \bar{C}_n(\gamma) \right) \exp\left(-\frac{4}{3\gamma^{3/2}} + 2\frac{A_n}{\sqrt{\gamma}} - \frac{2}{\beta} \right). \tag{8.5}$$

where $\Delta_2^2 = (\beta+1)/(\beta-1)$ and $|\bar{C}_n(\gamma)| < c_n\gamma$, for some $c_n > 0$. Hence $D_n > 0$.

The eigenfunction $w_n^{1,\sigma}$ has exactly n zeros in $[\bar{\chi}_n, 0]$.
The estimate (8.3) and the fact that Bi is uniformly bounded on $[\bar{\chi}_n, 0]$ imply that, for all $0 < \gamma < \gamma_0$ (with γ_0 small enough), the functions $w_0^{1,\sigma}$ and Ai are exponentially close in the W_∞^1-norm over that interval,

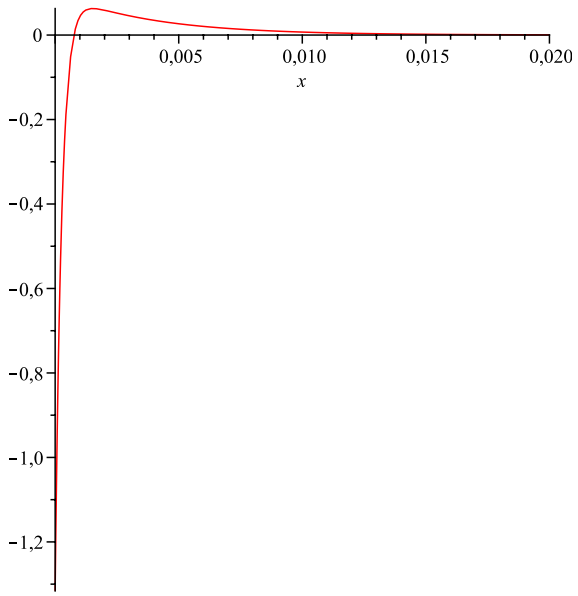

Figure 8.2: **Buoyant species** The function $w_0(x)$ has a maximum at $x_{\max}$ and has negative values in the beginning of the interval. Here, $\beta = -2$ and $\gamma = 0.01$.

$$\left\| w_n^{1,\sigma} + \mathrm{Ai} \right\|_{[\bar{\chi},0]} < c_n \exp\left(-\frac{4}{3\gamma^{3/2}} + 2\frac{|A_n|}{\sqrt{\gamma}} \right), \quad \text{for some} \quad c_n > 0. \tag{8.6}$$

As a result, we may use an argument exactly analogous to the one used in the proof of Lemma 7.4 to show that $w_n^{1,\sigma}$ has at least $n-1$ distinct zeros in that interval, each of which is exponentially close to one of $A_1, \ldots, A_{n-1}$. Also, observing that $\bar{\chi}_n$ is algebraically larger than A_n, by Lemmas 7.4 and A.2, while $w_n^{1,\sigma}$ is exponentially close to $-\mathrm{Ai}$, by estimate (6.4), we conclude that the zero of $w_n^{1,\sigma}$ close to A_n lies to the left of $\bar{\chi}_n$ and thus there are no other zeros in $[\bar{\chi}_n, \gamma^{-1} + \bar{\chi}_n]$.

It remains to show that there is a unique zero of $w_n^{1,\sigma}$ in $[0, \gamma^{-1} + \bar{\chi}_n]$. We show that $w_n^{1,\sigma}$ is increasing and changes sign in that interval. First, we calculate $(w_n^{1,\sigma})'(\chi) = D_n \mathrm{Bi}'(\chi) - \mathrm{Ai}'(\chi) > 0$, where we have used that $\mathrm{Bi}'(\chi) > 0$, $\mathrm{Ai}'(\chi) < 0$, and $D_n > 0$. Also, $w_n^{1,\sigma}(0) < 0$ (by $\mathrm{Ai} > 0$ and (8.4)) and, working as in section 8.1.1,

$$w_n^{1,\sigma}(\gamma^{-1} + \bar{\chi}_n) = \beta^{-1}\sqrt{\gamma}[D_n \mathrm{Bi}'(\gamma^{-1} + \bar{\chi}_n) - \mathrm{Ai}'(\gamma^{-1} + \bar{\chi}_n)] > 0.$$

This completes the proof.

The estimation D_n.
We show how we have derived D_0 using the Airy functions in Appendix A and 7.4

$$D_n = \frac{\Gamma_{R,n}(\mathrm{Ai})}{\Gamma_{R,n}(\mathrm{Bi})} = \frac{\Gamma(\mathrm{Ai}, \gamma^{-1} + \bar{\chi_n})}{\Gamma(\mathrm{Bi}, \gamma^{-1} + \bar{\chi_n})} = \frac{1}{2}\frac{\beta + \gamma^{1/2}(\gamma^{-1} + \bar{\chi}_n)^{1/2}}{\beta - \gamma^{1/2}(\gamma^{-1} + \bar{\chi}_n)^{1/2}} \exp\left(-\frac{4}{3}(\gamma^{-1} + \bar{\chi}_n)^{3/2}\right).$$

Using the estimates of Lemma 7.4 we find

$$\gamma^{-1} + \bar{\chi_n} = \gamma^{-1}\left(1 + \gamma A_n + \beta^{-1}\gamma^{3/2}\right).$$

Using Taylor's theorem we get

$$\begin{aligned} \left(\gamma^{-1} + \bar{\chi_n}\right)^{1/2} &= \gamma^{-1/2} + \frac{1}{2}\sqrt{\gamma}A_n + \frac{\gamma}{2\beta} \\ \left(\gamma^{-1} + \bar{\chi_n}\right)^{3/2} &= \gamma^{-3/2} + \frac{3A_n}{2\sqrt{\gamma}} + \frac{3}{2\beta}. \end{aligned}$$

Now we can write

$$D_n = \frac{1}{2}\frac{\beta + 1 + (1/2)(\gamma|A_n| + \beta^{-1}\gamma^{3/2})}{\beta - 1 - (1/2)(\gamma|A_n| + \beta^{-1}\gamma^{3/2})} \exp\left(\frac{-4}{3\gamma^{3/2}} + 2\frac{|A_n|}{\sqrt{\gamma}} - \frac{2}{\beta}\right).$$

We can rewrite D_n like in section 6.1.1. and we get the desired result. It follows that

$$|\bar{C}_n(\gamma)| < c_n\gamma \quad \text{for some} \quad c_n > 0.$$

8.2 The cases $0 < \beta < 1$ and $-1 < \beta < 0$

In this section, we select D_A and D_B so that (8.1) becomes

$$w_n^{1,\sigma}(\chi) = \mathrm{Ai}(\chi) + D_n\mathrm{Bi}(\chi), \quad \text{with} \quad D_n = -\frac{\Gamma_{R,n}(\mathrm{Ai})}{\Gamma_{R,n}(\mathrm{Bi})}. \tag{8.7}$$

In section 8.2.1 we show that the eigenfunction $w_n^{1,\sigma}$, $n = 0, \ldots, N$ has n zeros in the interval $[\bar{\chi}_n, \gamma^{-1} + \bar{\chi}_n]$, then we evaluate $\omega_0(x)$. In section 8.2.2 we determine the profiles for each case.

8.2.1 The eigenfunctions

The nth eigenvalue is $\mu_n^{1,\sigma} = -\gamma\sigma\bar{\chi}_n$, while the corresponding eigenfunction $w_0^{1,\sigma}$ is given by (8.7). An estimation of the constant D_n may be

$$D_n = \left(\frac{\Delta_3^2}{2} + \hat{C}_n(\gamma)\right) \exp\left(-\frac{4}{3\gamma^{3/2}} + 2\frac{|A_{n+1}|}{\sqrt{\gamma}} - \frac{2}{\beta}\right), \tag{8.8}$$

where $\Delta_3^2 = (1+\beta)/(1-\beta)$ and $|\hat{C}_n| < c_n'\gamma$, for some $c_n' > 0$. This estimate of D_n is of the same type as (8.5) but with A_n replaced by A_{n+1}.

The eigenfunction $w_n^{1,\sigma}$ has n zeros in the interval $[\bar{\chi}_n, \gamma^{-1} + \bar{\chi}_n]$.
The estimate (8.4) also holds here. Recalling that $\bar{\chi}_n$ is algebraically larger than A_{n+1}, we conclude that $w_n^{1,\sigma}$ has n distinct zeros each of which is exponentially close to one of $A_1, \ldots, A_n$. We show that $w_n^{1,\sigma} > 0$ in $[0, \gamma^{-1} + \bar{\chi}_n]$ and thus has no extra zeros. We calculate $w_n^{1,\sigma}(\chi) = \mathrm{Ai}(\chi) + D_n\mathrm{Bi}(\chi)$. Now, $\mathrm{Bi}(\chi) > 0$ and $\mathrm{Ai}(\chi) > 0$, for all $\chi \in [0, \gamma^{-1} + \bar{\chi}_n]$, while $D_n > 0$ by (8.6). Hence, $w_n^{1,\sigma} > 0$ and the proof is complete.

The solution ω_0.
Next we examine the profile of the solution ω_0 associated with w_0,

$$\omega_0(x) = C_{II}x^{1/4}\exp\left(\frac{\beta}{\gamma^{3/2}}x\right)\cosh(\theta_2(x)), \quad x \in [0,1], \tag{8.9}$$

where $C_{II} = (\pi^{-1/2})\gamma^{1/4}e^{(1/2)\psi_1}$, $|C_{II}| < c_{II}\gamma^{1/4}$ for some $c_{II} > 0$. The function ψ_1 is defined on page 54, and

$$\theta_2(x) = \frac{2}{3\gamma^{3/2}}\left(1 - x^{3/2}\right) - \left(\frac{|A_1|}{\sqrt{\gamma}} - \frac{1}{\beta}\right)(1 - \sqrt{x}) - \log\Delta_3.$$

We show how we derived ω_0 in four steps. First, we calculate

$$w_n^{1,\sigma}(\gamma^{-1}x + \bar{\chi}_n) = \mathrm{Ai}(\gamma^{-1}x + \bar{\chi}_n) + D_n\mathrm{Bi}(\gamma^{-1}x + \bar{\chi}_n),$$

where $\gamma^{-1}x + \bar{\chi}_n = \gamma^{-1}\left(x + \gamma A_n + \beta^{-1}\gamma^{3/2}\right)$. Then we use (6.1) to get ω_0. Using Taylor's Theorem we get

$$
\begin{aligned}
(\gamma^{-1}x + \bar{\chi}_n)^{-1/4} &= \gamma^{1/4}\left(x^{-1/4} - (1/4)x^{-5/4}(\gamma A_n + \beta^{-1}\gamma^{3/2})\right) \\
(\gamma^{-1}x + \bar{\chi}_n)^{3/2} &= (\gamma^{-1}x + \bar{\chi}_n)^{3/2} = \gamma^{-3/2}\left(x^{3/2} - (3/2)x^{1/2}(\gamma A_n + \beta^{-1}\gamma^{3/2})\right).
\end{aligned}
$$

Step 1

$$
\mathrm{Bi}(\gamma^{-1}x + \bar{\chi}_n) = \pi^{-1/2}\gamma^{1/4}x^{-1/4}\exp\left(\frac{2}{3\gamma^{3/2}}x^{3/2} + \frac{|A_1|}{\sqrt{\gamma}}\sqrt{x} + \frac{\sqrt{x}}{\beta}\right).
$$

Step 2

$$
D_0\mathrm{Bi}(\gamma^{-1}x + \bar{\chi}_n) = \left(\frac{\Delta_3^2}{2} + \hat{C}\right)\pi^{-1/2}\gamma^{1/4}x^{-1/4}\exp\left(\psi(x)\right).
$$

Rewriting the expression above we get

$$
D_0\mathrm{Bi}(\gamma^{-1}x + \bar{\chi}_n) = (1/2)(\pi^{-1/2}\gamma^{1/4}x^{-1/4})\exp\left(\psi(x)\right).
$$

with

$$
\begin{aligned}
\psi(x) &= -\frac{4}{3\gamma^{3/2}} + 2\frac{|A_1|}{\sqrt{\gamma}} - \frac{2}{\beta} + \frac{2}{3\gamma^{3/2}}x^{3/2} + \frac{|A_1|}{\sqrt{\gamma}}\sqrt{x} + \frac{\sqrt{x}}{\beta} \\
&= -\frac{4}{3\gamma^{3/2}} + \frac{2}{3\gamma^{3/2}}x^{3/2} + 2\frac{|A_1|}{\sqrt{\gamma}} + \frac{|A_1|}{\sqrt{\gamma}}\sqrt{x} - \frac{2}{\beta} + \frac{\sqrt{x}}{\beta} + \log\Delta_3^2.
\end{aligned}
$$

Step 3

$$
\mathrm{Ai}(\gamma^{-1}x + \bar{\chi}_n) = (1/2)\pi^{-1/2}\gamma^{-1/4}\exp\left(-\frac{2}{3\gamma^{3/2}}x^{3/2} - \frac{|A_1|}{\sqrt{\gamma}}\sqrt{x} - \frac{\sqrt{x}}{\beta}\right).
$$

Step 4

To make calculations easier we write

$$
\begin{aligned}
\psi_0(x) &= \frac{2}{3\gamma^{3/2}}x^{3/2} + \frac{|A_1|}{\sqrt{\gamma}}\sqrt{x} + \frac{\sqrt{x}}{\beta} \\
\psi_1 &= -\frac{4}{3\gamma^{3/2}} + 2\frac{|A_1|}{\sqrt{\gamma}} - \frac{2}{\beta} + \log\Delta_3^2
\end{aligned}
$$

and $\psi(x) = \psi_0(x) + \psi_1$. Then

$$\begin{aligned} \mathrm{Ai}(\gamma^{-1}x + \bar{\chi}_n) + D_0\mathrm{Bi}(\gamma^{-1}x + \bar{\chi}_n) &= (1/2)\pi^{-1/2}\gamma^{1/4}x^{-1/4}\left(e^{-\psi_0} + e^{\psi_0+\psi_1}\right) \\ &= \pi^{-1/2}\gamma^{1/4}x^{-1/4}e^{(1/2)\psi_1}\cosh\left(\theta_2(x)\right), \end{aligned}$$

where $\theta_2(x) = (1/2)(e^{(\psi_0+(1/2)\psi_1)} + e^{(-(\psi_0)+(1/2)\psi_1)})$. Thus

$$w_n^{1,\sigma} = C_{II}x^{-1/4}\cosh(\theta_2(x)),$$

where $C_{II} = \pi^{-1/2}\gamma^{1/4}e^{(1/2)\psi_1}$ and $\theta_2(x)$ is the following expression

$$\theta_2(x) = \frac{2}{3\gamma^{3/2}}(x^{3/2} - 1) + \frac{|A_1|}{\sqrt{\gamma}}(1 + \sqrt{x}) + \frac{1}{\beta}(\sqrt{x} - 1) + \log\Delta_3.$$

Using (6.1) we find $\omega_0(x)$.

8.2.2 The profiles

The profiles for $0 < \beta < 1$, sinking species

The function $\omega_0(x)$ has a spike around the point

$$|x_\beta - (\beta^2 + |A_1|\gamma)| < c\gamma^2, \quad \text{for some} \quad c > 0. \tag{8.10}$$

Figure 8.3 shows the graph of $\omega_0(x)$.

The profile for $-1 < \beta < 0$, buoyant species

For all $x \in [0, 1]$ $\omega_0 > 0$. To leading order we can write ω_0 as

$$\omega_0 = \mathrm{cexp}\left(\frac{\beta}{\gamma^{3/2}}x\right)\cosh\left(\frac{1}{\gamma^{3/2}}(x^{2/3} - 1) + \frac{|A_1|}{\sqrt{\gamma}}(1 + \sqrt{x})\right), \quad \text{where} \quad c > 0.$$

Thus, the function $\omega_0(x)$ corresponds with a boundary layer at $x = 0$, see Figure 8.4.

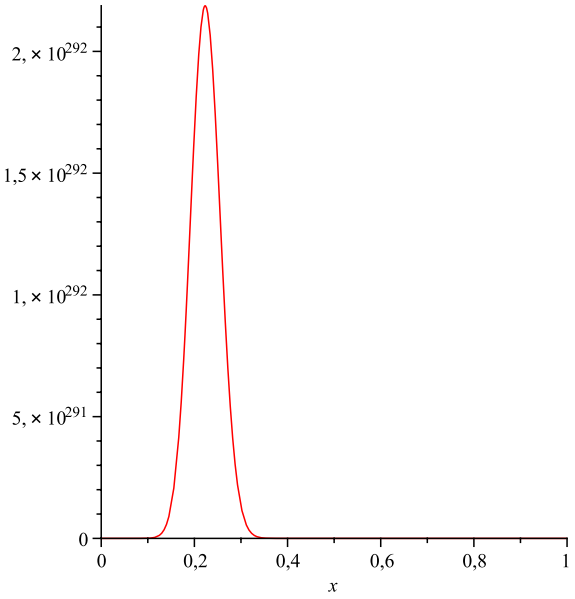

Figure 8.3: **Sinking species** The function $w_0(x)$ has a spike around the point x_β. Here, $\beta = 0.5$ and $\gamma = 0.01$.

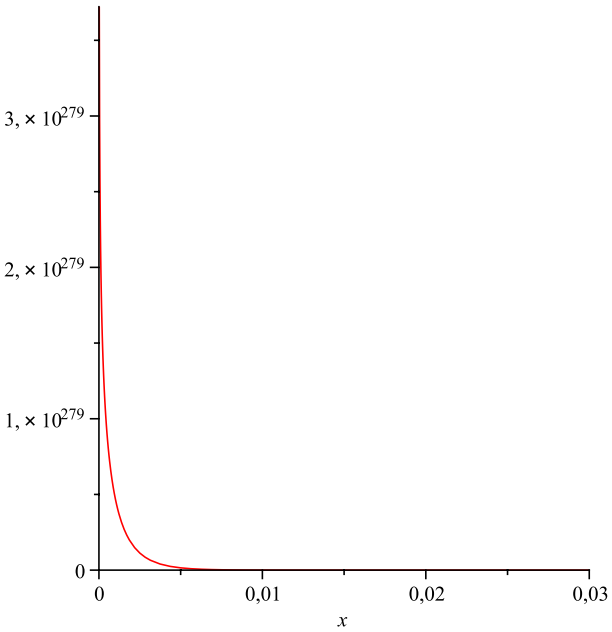

Figure 8.4: **Buoyant species** The function $w_0(x)$ corresponds to a boundary layer at $x = 0$. Here, $\beta = -0.5$ and $\gamma = 0.01$.

Chapter 9

The WKB approximation

In this section we use the WKB method to derive explicit, though asymptotic, formulas for the eigenvalues $\mu_1, \ldots, \mu_n$ of $\mathcal{L}$. In section 9.1 we derive the formulas for the eigenfunctions for the case $a^2/4 < \sigma_L$, and in section 9.2 for the case $a^2/4 > \sigma_U$. We study the profiles and determine the structure of the phytoplankton patterns corresponding to the profiles. In section 9.3 we deal with the transitional regime $\sigma_L < a^2/4 < \sigma_U$. The structure of the phytoplankton patterns for sinking and buoyant species are:

The case $a^2/4 < \sigma_L$.

- Sinking species $0 < \beta < 1$: Deep Chlorophyll Maximum.
- Buoyant species $-1 < \beta < 0$: Surface Layer.

The case $a^2/4 > \sigma_U$.

- Sinking species $\beta > 1$: Benthic Layer.
- Buoyant species $\beta < -1$: unknown structure.

9.1 The case $a^2/4 < \sigma_L$

In section 9.1.1 we derive the WKB formulas for the eigenvalue problem (6.2). In section 9.1.2 we determine the boundary conditions for the WKB formulas. We determine the eigenvalues of (4.13) in section 9.1.3 and the eigenfunctions in section 9.1.4. In section 9.1.5. we determine the profiles for $a < 0$ and $a > 0$.

9.1.1 WKB formulas for w

The eigenvalue problem (6.2) reads

$$\varepsilon w_{xx} = (F(x) - \mu)w, \quad \text{with} \quad \mathcal{G}(w,0) = \mathcal{G}(w,1) = 0 \tag{9.1}$$

Lemma 6.3 states that the eigenvalues $\mu_1, \ldots, \mu_n$ lie in a $\mathcal{O}(\varepsilon^{1/3})$ region to the right of zero. Thus for any $0 \le n \le N$

$$F(x) < \mu_n, \quad \text{for} \quad x \in [0, \bar{x}_n), \quad \text{and} \quad F(x) > \mu_n, \quad \text{for} \quad x \in (\bar{x}_n, 1].$$

Here, $\bar{x}_n$ corresponds to a turning point, i.e., $F(\bar{x}_n) = \mu_n$, and it is given by

$$\bar{x}_n = \frac{1}{\kappa} \log \frac{1 + \mu_n(1+\eta_H)(1+j_H^{-1})}{1 - \mu_n(1+\eta_H)(1+j_H^{-1})}. \tag{9.2}$$

Using Lemmas 6.3 and A.2 the eigenvalue μ_n may be expanded asymptotically in powers of $\varepsilon^{1/6}$ starting with $\mathcal{O}(\varepsilon^{1/3})$ terms,

$$\begin{aligned}
\mu_n^{1,\sigma} &= \mu_{n+1}^{*,\sigma} + C_{n+1}\delta_{n+1,\sigma} \\
&= \lambda^* - \lambda_{n+1}^{*,\sigma} + C_{n+1}\varepsilon^{1/6}\exp\left((-4/3)\sqrt{\sigma/\varepsilon} + 2|A_{n+1}|(\sigma/\varepsilon)^{1/6}\right) \\
&= \varepsilon^{1/3}\sigma^{2/3}|A'_{n+1,\sigma}| + C_{n+1}\varepsilon^{1/6}\exp(\nu_{\sigma,\varepsilon}) \\
&= \varepsilon^{1/3}\sigma^{2/3}(A_{n+1} + \beta^{-1}\varepsilon^{1/6}\sigma_n^{-1/6} + c_a\varepsilon^{1/3}\sigma_n^{-1/3}) + C_{n+1}\varepsilon^{1/6}\exp(\nu_{\sigma,\varepsilon}) \\
&= (\sigma^{2/3}A_{n+1})\varepsilon^{1/3} + (\beta^{-1}\sigma^{2/3})\varepsilon^{1/2} + (\sigma^{2/3}c_a)\varepsilon^{2/3} + C_{n+1}\varepsilon^{1/6}\exp(\nu_{\sigma,\varepsilon})
\end{aligned}$$

where $\nu_{\sigma,\varepsilon} = (-4/3)\sqrt{\sigma/\varepsilon} + 2|A_{n+1}|(\sigma/\varepsilon)^{1/6}$. From this asymptotic expansion we see that we can write $\mu_n^{1,\sigma}$ as $\mu_n = \sum_{\ell=2}^{\infty} \varepsilon^{l/6}\mu_{n,\ell}$. Thus, we also find

$$\bar{x}_n = \varepsilon^{1/3}\sigma_0^{-1}\mu_{n,2} + \varepsilon^{1/2}\sigma_0^{-1}\mu_{n,3} + \mathcal{O}(\varepsilon^{2/3}), \quad \text{where} \quad \sigma_0 = F'(0).$$

First, we determine the solution in the region $x \in (\bar{x}_n, 1]$, and then in the region $x \in [0, \bar{x}_n)$.

The solution in the region $x \in (\bar{x}_n, 1]$.
The solution in this region, where $F(x) - \mu_n > 0$, can be determined using standard formulas,

$$w_n(x) = [F(x) - \mu_n]^{-1/4} \left[C_a e^{-\int_{\bar{x}_n}^x \sqrt{(F(s)-\mu_n)/\varepsilon}\ ds} + C_b e^{\int_{\bar{x}_n}^x \sqrt{(F(s)-\mu_n)/\varepsilon}\ ds} \right]. \quad (9.3)$$

Here, C_a and C_b are arbitrary constants, to leading order in ε. Using this information and the asymptotic expansion for μ_n, we may determine the principal part of the solution w_n,

$$w_{n,0}(x) = [F(x)]^{-1/4} \left[C_{a,0} e^{-\theta_3(x)} + C_{b,0} e^{\theta_3(x)} \right], \quad (9.4)$$

for arbitrary constants $C_{a,0}$ and $C_{b,0}$, and

$$\theta_3(x) = \frac{1}{\varepsilon^{1/2}} \int_0^x \sqrt{F(s)} ds - \frac{1}{\varepsilon^{1/6}} \frac{\mu_{n,2}}{2} \int_0^x \frac{1}{\sqrt{F(s)}} ds + (1/3)\sigma_0^{-1}(\mu_{n,2})^{3/2} - \frac{\mu_{n,3}}{2} \int_0^x \frac{1}{\sqrt{F(s)}} ds. \quad (9.5)$$

Before determining the solution in the region $[0, \bar{x}_n)$, we show how $\theta_3(x)$ is evaluated. We start by evaluating $\int_{\bar{x}_n}^x \sqrt{(F(s)-\mu_n)/\varepsilon}\ ds$ in (9.4). Since μ_n is very small we can write $\sqrt{F(s)-\mu_n} = \sqrt{F(s)} - \frac{\mu_n}{2} \frac{1}{\sqrt{F(s)}}$,

$$\begin{aligned} \frac{1}{\varepsilon^{1/2}} \int_{\bar{x}_n}^x \sqrt{F(s)-\mu_n} ds &= \varepsilon^{-1/2} \int_{\bar{x}_n}^x \sqrt{F(s)} ds - \varepsilon^{-1/2} \frac{\mu_n}{2} \int_{\bar{x}_n}^x \frac{1}{\sqrt{F(s)}} ds \\ &= \frac{1}{\varepsilon^{1/2}} \int_0^x \sqrt{F(s)} ds - \frac{1}{\varepsilon^{1/2}} \int_0^{\bar{x}_n} \sqrt{F(s)} ds - \frac{1}{\varepsilon^{1/2}} \frac{\mu_n}{2} \int_0^x \frac{1}{\sqrt{F(s)}} ds \\ &\quad + \frac{1}{\varepsilon^{1/2}} \frac{\mu_n}{2} \int_0^{\bar{x}_n} \frac{1}{\sqrt{F(s)}} ds. \end{aligned}$$

We evaluate the last three terms of the integral in (9.6):

The second term
We write $F(s) = s\sigma_0$. Using Taylor's Theorem we obtain

$$-\frac{1}{\varepsilon^{1/2}} \int_0^{\bar{x}_n} \sqrt{s\sigma_0} ds = (\varepsilon^{-1/2})(2/3)\sigma_0^{-1}\varepsilon^{1/2}(\mu_{n,2})^{3/2} = -(2/3)\sigma_0^{-1}(\mu_{n,2})^{2/3}.$$

The third term

$$-\frac{1}{\varepsilon^{1/2}} \frac{\mu_n}{2} \int_0^x \frac{1}{\sqrt{F(s)}} ds = -\frac{1}{\varepsilon^{1/6}} \frac{\mu_{n,2}}{2} \int_0^x \frac{1}{\sqrt{F(s)}} ds - \frac{\mu_{n,3}}{2} \int_0^x \frac{1}{\sqrt{F(s)}} ds.$$

The fourth term
Again we use $F(s) = s\sigma_0$,

$$\int_0^{\bar{x}_n} \frac{1}{\sqrt{s\sigma_0}} ds = 2\varepsilon^{1/6}\sigma_0^{-1}\sqrt{\mu_{n,2}}.$$

Multiplying this integral times $\varepsilon^{-1/2}(\varepsilon^{1/3}\mu_{n,2})$ we find that the fourth term is $\sigma_0^{-1}(\mu_{n,2})^{3/2}$.

The solution in the region $[0, \bar{x}_n)$.
To determine this solution, we change independent variable through

$$x = \varepsilon^{1/3}\sigma_0^{-1/3}(\chi - \bar{\chi}_n), \quad \text{where} \quad \bar{\chi}_n = -\sigma_0^{1/3}\varepsilon^{-1/3}\bar{x}_n = -\sigma_0^{-2/3}\mu_{n,2} - \mathcal{O}(\varepsilon^{1/6}) < 0, \tag{9.6}$$

and expand $F(x) - \mu_n$ asymptotically. We recall that $F(0) = 0$ and $F'(0) = \sigma_0$, so that

$$\begin{aligned} F(x) &= F(\varepsilon^{1/3}\sigma_0^{-1/3}(\chi - \bar{\chi}_n)) \\ &= F(0) + \varepsilon^{1/3}\sigma_0^{-1/3}(\chi - \bar{\chi}_n)F'(0) \\ &= \varepsilon^{1/3}\sigma_0^{2/3}(\chi - \bar{\chi}_n) \\ &= \varepsilon^{1/3}\sigma_0^{2/3}\chi - \varepsilon^{1/3}\sigma_0^{2/3}(-\sigma_0^{-2/3}\mu_{n,2} - \mathcal{O}(\varepsilon^{1/6})) \\ &= \varepsilon^{1/3}\sigma_0^{2/3}\chi + \mathcal{O}(\varepsilon^{1/3}), \end{aligned}$$

Thus

$$F(x) - \mu_n = F(\varepsilon^{1/3}\sigma_0^{-1/3}(\chi - \bar{\chi}_n)) - \mu_n = \varepsilon^{1/3}\sigma_0^{2/3}\chi. \tag{9.7}$$

As a result, (9.1) becomes, to leading order, the Airy equation $(w_n)_{\chi\chi} = \chi w_n$, hence

$$w_{n,0}(\chi) = D_{a,0}\mathrm{Ai}(\chi) + D_{b,0}\mathrm{Bi}(\chi), \quad \text{with} \quad \chi \in (-\sigma_0^{-2/3}\mu_{n,2}, 0]. \tag{9.8}$$

9.1.2 Boundary conditions for the WKB solution

In this section we determine the coefficients $C_{a,0}$,$C_{b,0}$, $C_{b,0}$, and $C_{b,0}$ appearing in (9.5) and (9.9). First, we determine the boundary condition for the formula

in (9.5), then for the formula in (9.9). Using matching we find the boundary conditions.

Boundary condition for the formula (9.5)

Formula $w_{n,0}(x)$ in (9.5) represents the solution in region $(\bar{x}_n, 1]$, and thus it must satisfy the boundary condition at $x = 1$, $\mathcal{G}(w_n, 1) = 0$. Using (6.3) we find, to leading order,

$$C_{a,0}(a + 2\sqrt{\sigma_1})e^{-\theta_3(1)} + C_{b,0}(a - 2\sqrt{\sigma_1})e^{\theta_3(1)} = 0, \quad \text{where} \quad \sigma_1 = F(1). \tag{9.9}$$

In order to find (9.10) we need to evaluate

$$\mathcal{G}(w, x) = w(x) - \frac{2\sqrt{\varepsilon}}{a} w_x(x),$$

where we write $w := w_{n,0}(x)$ for simplicity. Differentiating w we get

$$\begin{aligned} w_x(x) &= [F(x)]^{-1/4}[-\theta_3'(x)C_{a,0}e^{-\theta_3(x)} + \theta_5'(x)C_{b,0}e^{\theta_5(x)}] \\ &\quad -(1/4)[F(x)]'[F(x)]^{-5/4}[C_{a,0}e^{-\theta_3(x)} + C_{b,0}e^{\theta_3(x)}], \end{aligned}$$

where $\theta_3'(x) = \varepsilon^{-1/2}\frac{d}{dx}\int_0^x \sqrt{F(s)}ds = \sqrt{F(x)}$. Thus

$$\begin{aligned} \mathcal{G}(w, x) &= [F(x)]^{-1/4}[C_{a,0}e^{-\theta_3(x)} + C_{b,0}e^{\theta_3(x)}] \\ &\quad -\frac{2}{a}[F(x)]^{-1/4}[-\sqrt{F(x)}C_{a,0}e^{-\theta_3(x)} + \sqrt{F(x) - \mu_{0,0}}C_{b,0}e^{\theta_3(x)}], \end{aligned}$$

and

$$\mathcal{G}(w_n, 1) = a[C_{a,0}e^{-\theta_3(1)} + C_{b,0}e^{\theta_3(1)}] + 2[\sqrt{\sigma_1}C_{a,0}e^{-\theta_3(1)} - \sqrt{\sigma_1}C_{b,0}e^{\theta_3(1)}] = 0.$$

Rearranging the terms gives (9.10).

Boundary condition for the formula (9.9)

The formula given in (9.9) is valid for $\chi \in (-\sigma_0^{-2/3}\mu_{n,2}, 0]$ (equivalently, for $x \in [0, \bar{x}_n)$), and it must therefore satisfy the boundary condition $\mathcal{G}(w, 0) = 0$. Recasting the formula for $\mathcal{G}$ given in (6.3) in terms of χ, we obtain to leading order

$$D_{a,0}\mathrm{Ai}(-\sigma_0^{-2/3}\mu_{n,2}) + D_{b,0}\mathrm{Bi}(-\sigma_0^{-2/3}\mu_{n,2}) = 0. \tag{9.10}$$

Matching
We set $\psi = \varepsilon^{-d}(x - \bar{x})$, where $1/5 < d < 1/3$, and recast (9.5) in terms of ψ. We find, to leading order and for all $\mathcal{O}(1)$, positive values of ψ,

$$w_{n,0}(x(\psi)) = \varepsilon^{-d/4}\sigma_0^{-1/4}\psi^{-1/4}\left[C_{a,0}e^{-\theta_4(\psi)-(1/3)\sigma_0^{-1}(\mu_{n,2})^{3/2}} + C_{b,0}e^{\theta_4(\psi)+(1/3)\sigma_0^{-1}(\mu_{n,2})^{3/2}}\right],$$

where $\theta_4(\psi) = (2/3)\varepsilon^{(3d-1)/2}\sqrt{\sigma_0}\psi^{3/2}$. Similarly, (9.9) yields

$$w_{n,0}(x(\psi)) = \varepsilon^{1/12-d/4}\sigma_0^{-1/12}\pi^{-1/2}\psi^{-1/4}\left[(1/2)D_{a,0}e^{-\theta_4(\psi)} + D_{b,0}e^{\theta_4(\psi)}\right].$$

The matching condition around the turning point gives, then

$$C_{a,0} = \varepsilon^{1/12}\frac{\sigma_0^{1/6}}{2\sqrt{\pi}}e^{\sigma_0^{-1}(\mu_{n,2})^{3/2}}D_{a,0} \quad \text{and} \quad C_{b,0} = \varepsilon^{1/12}\frac{\sigma_0^{1/6}}{\sqrt{\pi}}e^{-\sigma_0^{-1}(\mu_{n,2})^{3/2}}D_{b,0} \tag{9.11}$$

9.1.3 The eigenvalues $\mu_0, \ldots, \mu_n$

In this chapter we derive the eigenvalues of (4.13). The linear system (9.10)-(9.12) has a nontrivial solution if and only if the determinant corresponding to it vanishes identically,

$$-2(a - 2\sqrt{\sigma_1})\exp(\bar{\theta}_3)\mathrm{Ai}(-\sigma_0^{-2/3}\mu_{n,2}) + (a + 2\sqrt{\sigma_1})\exp(-\bar{\theta}_3)\mathrm{Bi}(-\sigma_0^{-2/3}\mu_{n,2}) = 0.$$

where $\bar{\theta}_3 = \theta_3(1) - \sigma_0^{-1}(\mu_{n,2})^{3/2}$. Since $F(s) \geq \sigma_L$s (see (5.2)), we have

$$\theta_3(1) = \varepsilon^{-1/2}\int_{\bar{x}_n}^1 \sqrt{F(s)}ds \geq \varepsilon^{-1/2}\int_{\bar{x}_n}^1 \sqrt{\sigma_L s}ds = \mathrm{c}\varepsilon^{-1/2}\sqrt{\sigma_L},$$

where $c = (2/3) - (\bar{x}_n)^{3/2}$, thus $\theta_3(1) \geq \mathcal{O}(\varepsilon^{-1/2})$. We see that the determinant condition reduces to $\mathrm{Ai}(-\sigma_0^{-2/3}\mu_{n,2}) = 0$, hence $\mu_{n,2} = \sigma_0^{2/3}A_n = \sigma_0^{2/3}|A_n| > 0$. Thus we find for the eigenvalues of (4.13),

$$\lambda_n = \lambda^* - \varepsilon^{1/3}\sigma_0^{2/3}|A_n| + \mathcal{O}(\varepsilon^{1/2}). \tag{9.12}$$

Recalling that $\sigma_0 = F'(0) = -f'(0)$ by (5.1) and Lemma 5.1, we find that the WKB formula (9.13) coincides - up to and including terms of $\mathcal{O}(1)$ and $\mathcal{O}(\varepsilon^{1/3})$ - for
(a) $0 < j_H < j_H^{(2)}$, with the rigorous lower bound for λ_n in Theorem 5.1,

(b) $j_H > 1$, with the rigorous upper bound for λ_n in Theorem 5.1.

For the remaining values of j_H, (9.13) yields a value for λ_n which lies in between the rigorous bounds derived in Theorem 5.1. In that case, $\sigma_L < F'(0) < \sigma_U$.

9.1.4 The eigenfunctions $w_0, \ldots, w_n$

The principal part of w_n is given by the formula

$$w_{n,0}(x) = \begin{cases} \mathrm{Ai}(A_n + \varepsilon^{-1/3}\sigma_0^{1/3}x), & \text{for } x \in [0, \varepsilon^{1/3}\sigma_0^{-1/3}|A_n|), \\ C[F(x)]^{-1/4}\cosh\Theta(x), & \text{for } x \in (\varepsilon^{1/3}\sigma_0^{-1/3}|A_n|, 1]. \end{cases} \tag{9.13}$$

Here

$$C = \varepsilon^{1/12}\frac{\sigma_0^{1/6}}{\sqrt{\pi}}\Delta_4 e^{|A_n|^{3/2}-\theta_3(1)}, \quad \text{where } \Delta_4^2 = \frac{2\sqrt{\sigma_1}+a}{2\sqrt{\sigma_1}-a}, \tag{9.14}$$

and

$$\Theta(x) = \varepsilon^{-1/2}\int_x^1 \sqrt{F(s)}ds - \left(\varepsilon^{-1/6}\frac{\sigma_0^{2/3}|A_n|}{2} - \frac{\sigma_0}{a}\right)\int_x^1 \frac{1}{\sqrt{F(s)}}ds + \log\Delta_4 \tag{9.15}$$

Evaluation of $w_{n,0}(x)$
Substituting

$$C_{b,0} = \frac{2\sqrt{\sigma_1}+a}{2\sqrt{\sigma_1}-a}e^{-2\theta_3(1)}C_{a,0}.$$

in (9.5) we get

$$\begin{aligned} w_{n,0}(x) &= [F(x)]^{-1/4} C_{a,0} \left[e^{-\theta_3(x)} + \Delta_4^2 e^{-2\theta_3(1)} e^{\theta_3(x)} \right] \\ &= [F(x)]^{-1/4} \varepsilon^{1/12} \frac{\sigma_0^{1/6}}{2\sqrt{\pi}} e^{\sigma_0^{-1}(\mu_{n,2})^{3/2}} D_{a,0} \left[e^{-\theta_3(x)} + e^{\theta_3(x)+\log\Delta_4^2-2\theta_3(1)} \right] \\ &= [F(x)]^{-1/4} \varepsilon^{1/12} \frac{\sigma_0^{1/6}}{2\sqrt{\pi}} \Delta_4 e^{|A_n|^{3/2}-\theta_3(1)} D_{a,0} \left[e^{\theta_3(x)+\log\Delta_4-\theta_3(1)} + e^{-(\theta_3(x)+\log\Delta_4-\theta_3(1))} \right] \\ &= C[F(x)]^{-1/4} D_{a,0} \cosh\left(\theta_3(x) + \log\Delta_4 - \theta_3(1)\right). \end{aligned}$$

In order to calculate $\theta_3(x) - \theta_3(1)$ we use (9.6),

$$\theta_3(x) - \theta_3(1) = \varepsilon^{-1/2} \int_1^x \sqrt{F(s)} ds - \left(\varepsilon^{-1/6} \frac{\sigma_0^{2/3}|A_n|}{2} - \frac{\sigma_0}{a} \right) \int_1^x \frac{1}{\sqrt{F(s)}} ds.$$

where $\mu_{n,2} = \sigma_0^{2/3}|A_n|$ and $\mu_{n,3} = -2\sigma_0/a$. Thus $e^{\theta_3(x)+\log\Delta_4-\theta_3(1)}$ can be written as

$$\exp\left[\varepsilon^{1/2} \int_1^x \sqrt{F(s)} ds - \left(\varepsilon^{-1/6} \frac{\sigma_0^{2/3}|A_n|}{2} - \frac{\sigma_0}{a} \right) \int_1^x \frac{1}{\sqrt{F(s)}} ds + \log\Delta_4 \right].$$

Recalling (6.1), we find

$$\omega_{n,0}(x) = \begin{cases} e^{ax/2\sqrt{\varepsilon}} \mathrm{Ai}(A_n + \varepsilon^{-1/3}\sigma_0^{1/3} x), & \text{for } x \in [0, \varepsilon^{1/3}\sigma_0^{-1/3}|A_n|), \\ C[F(x)]^{-1/4} e^{ax/2\sqrt{\varepsilon}} \cosh\Theta(x), & \text{for } x \in (\varepsilon^{1/3}\sigma_0^{-1/3}|A_n|, 1]. \end{cases} \quad (9.16)$$

9.1.5 The profiles for $a^2/4 < \sigma_L$.

In this section we will study the function $\omega_{0,0}$ in (9.17) for $0 < \beta < 1$ and for $-1 < \beta < 0$. In order to analyse $\omega_{0,0}$ we will insert parameters. We choose $\eta_H = 0.667$, $j_H = 0.5$, and $\kappa = 1$. Let us recall from chapter 5 that

$$F(x) = \frac{j_H(e^{\kappa x} - 1)}{(1+\eta_H)(1+j_H)(1+j_H e^{\kappa x})}.$$

With the chosen parameters the function $F(x)$ becomes

$$F(x) = \frac{e^x - 1}{5 + 2.5e^x}.$$

Further, $\sigma_0 = F'(0) = 0.1333$ and $\sigma_1 = F(1) = 0.1456$. Since $\bar{x}_0 = \varepsilon^{1/3}\sigma_0^{-1}\mu_{0,2} = \varepsilon^{1/3}\sigma_0^{-1/3}|A_0| \approx 0.027$, and $\theta_3(1) = \varepsilon^{-1/2}\int_{\bar{x}_0}^{x}\sqrt{F(s)}ds$, we have

$$\theta_3(1) = \frac{1}{\varepsilon^{1/2}}\int_{0.027}^{x}\sqrt{F(s)}ds.$$

Since $a^2/4 < \sigma_L = 0.1333$, we must choose $0 < a < 0.7302$ for $a > 0$, and $-0.7302 < a < 0$ for $a < 0$. We insert the following parameters in the function $\omega_{0,0}(x)$

$$\begin{aligned}
\sigma_0 &= 0.1333\\
\sigma_1 &= 0.1456\\
\eta_H &= 0.667\\
j_H &= 0.5\\
\kappa &= 1\\
\varepsilon &= 2\cdot 10^{-7}
\end{aligned}$$

With the chosen parameters the function $\omega_{0,0}(x)$ becomes

$$\omega_{0,0}(x) = C\left(\frac{e^x-1}{5+2.5e^x}\right)^{-1/4} e^{ax/2\sqrt{\varepsilon}}\cosh\left(\Theta(x)\right),$$

where

$$C = \frac{\varepsilon^{1/12}(0.1333)^{1/6}}{2\sqrt{\pi}}\frac{\sqrt{0.7632+a}}{\sqrt{0.7632-a}}\exp\left((2.3381)^{2/3} - 2236\int_{0.027}^{1}\sqrt{F(s)}ds\right), \quad \text{and}$$

$$\Theta(x) = \frac{1}{\varepsilon^{1/2}}\int_1^x\sqrt{F(s)}ds - \left(\frac{(0.1333)^{2/3}2.3381}{2\varepsilon^{1/6}} - \frac{0.1333}{a}\right)\int_x^1\frac{1}{\sqrt{F(s)}}ds + \ln\left(\frac{\sqrt{0.7632+a}}{\sqrt{0.7632-a}}\right).$$

The profile for $a > 0$ (or equivalently $0 < \beta < 1$), sinking species

Differentiating $\omega_{0,0}$ we find that the function has a spike around the point

$$x_{\mathrm{DCM}} = x_{\mathrm{DCM},0} + \mathcal{O}(\varepsilon^{1/3}) \tag{9.17}$$

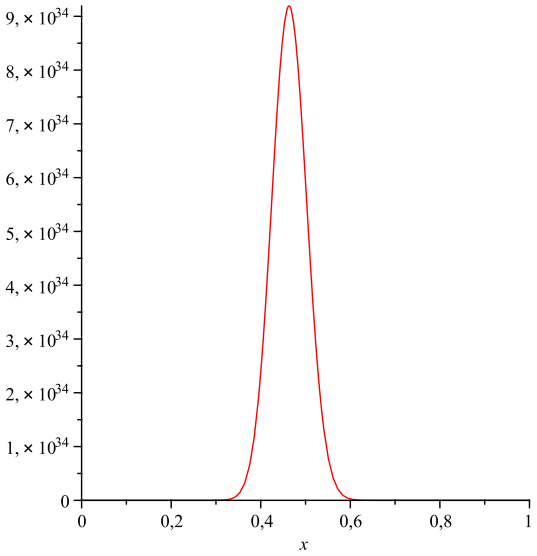

Figure 9.1: **Sinking species** The eigenfunction ω_0 corresponds to a DCM. Here $a = 0.5$, $\sigma_0 = 0.1333$, $\sigma_1 = 0.1456$, $\eta_H = 0.667$, $\varepsilon = 2{\cdot}10^{-7}$, $\kappa = 1$, and $j_H = 0.5$.

where $x_{\mathrm{DCM},0}$ is the unique solution to $F(x_{\mathrm{DCM},0}) = a^2/4$. Thus $\omega_{0,0}$ corresponds to a DCM, see Figure 9.1.

The profile for $a < 0$ (or equivalently $-1 < \beta < 0$), buoyant species

To leading order we can write

$$\omega_{0,0} = c_1\, e^{\frac{ax}{2}+\int_1^x \sqrt{F(s)}ds} - c_1\, e^{\frac{ax}{2}-\int_1^x \sqrt{F(s)}ds}.$$

The function $\frac{ax}{2} - \int_1^x \sqrt{F(s)}\mathrm{ds}$ is negative on the interval $[0,1]$, we can therefore neglect the second term in the equation above. The function $\frac{ax}{2} + \int_1^x \sqrt{F(s)}\mathrm{ds}$ is a descending on the interval $[0,1]$. Thus, $\omega_{0,0}$ corresponds to a SL, see Figure 9.2.

9.2 The case $a^2/4 > \sigma_U$

In this chapter we determine the eigenvalues and eigenfunctions for $a^2/4 > \sigma_U$ in section 9.2.1. In section 9.2.2 we study the profiles for $a > 0$ and $a < 0$.

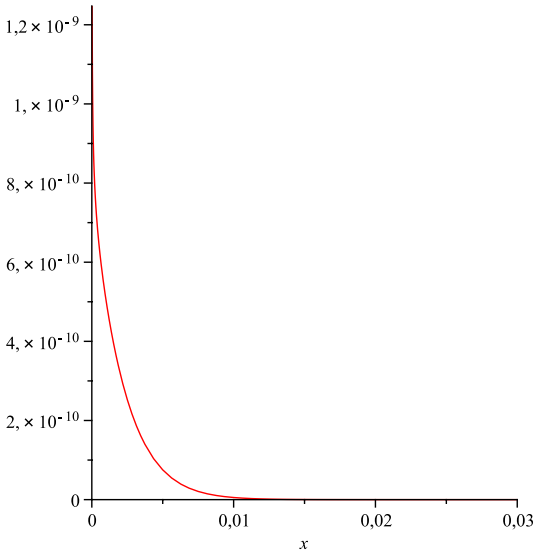

Figure 9.2: **Buoyant species** The eigenfunction ω_0 corresponds to a SL. Here $a = -0.5$, $\sigma_0 = 0.1333$, $\sigma_1 = 0.1456$, $\eta_H = 0.667$, $\varepsilon = 2 \cdot 10^{-7}$, $\kappa = 1$, and $j_H = 0.5$.

9.2.1 Eigenvalues and eigenfunctions

Here, the eigenvalue problem (6.2) also has the form (9.1). Since $a^2/4 > \sigma_U$, the eigenvalue μ_0 is $\mathcal{O}(1)$ and negative. The eigenvalues $\mu_1, \ldots, \mu_N$ are $\mathcal{O}(\varepsilon^{1/3})$ and positive.
Due to the qualitative difference between μ_0 and the eigenvalues of higher order, we consider them separately.

The case $1 \leq n \leq N$

For each such n, the eigenvalue problem (9.1) has a unique turning point $\bar{x}_n$ given by (9.2). The analysis in the preceding section applies here also. The formulas for μ_n and ω_n, $1 \leq n \leq N$, are identical to those of the preceding section, the only modification is that A_n in (9.13)-(9.16) must be replaced by A_{n-1}. This completes the analysis for the case $1 \leq n \leq N$.

The case $n = 0$

Since $\mu_0 < 0 < F(x)$ for all $x \in [0, 1]$, the eigenvalue problem (9.1) corresponding to μ_0 has no turning points. Thus the WKB formula (9.4) with $n = 0$ and $\bar{x}_n$ replaced by zero, is valid for all $x \in [0, 1]$. Lemmas 6.3 and A.2 suggest that μ_0 may be expanded asymptotically as $\mu_0 = \sum_{\ell=0}^{\infty} \varepsilon^{l/2} \mu_{0,\ell}$. Using this expansion, we calculate the principal part of w_0,

$$w_{0,0}(x) = [F(x) - \mu_{0,0}]^{-1/4} \left[C_{a,0} e^{-\theta_5(x)} + C_{b,0} e^{\theta_5(x)} \right], \tag{9.18}$$

where $C_{a,0}$ and $C_{b,0}$ are arbitrary constants and

$$\theta_5(x) = \frac{1}{\varepsilon^{1/2}} \int_0^x \sqrt{F(s) - \mu_{0,0}} ds - \frac{\mu_{0,1}}{2} \int_0^x \frac{1}{\sqrt{F(s) - \mu_{0,0}}} ds. \tag{9.19}$$

In the WKB formula we need to determine $\int_0^x \sqrt{F(s) - \mu_{0,0} - \varepsilon^{1/2}\mu_{0,1}} ds$. Since $\varepsilon^{1/2}\mu_{0,1}$ is very small, we use Taylor's theorem to rewrite this integral,

$$\int_0^x \sqrt{F(s) - \mu_{0,0} - \varepsilon^{1/2}\mu_{0,1}} ds = \int_0^x \sqrt{F(x) - \mu_{0,0}} ds - \frac{\mu_{0,1}\varepsilon^{1/2}}{2} \int_0^x \sqrt{F(x) - \mu_{0,0}} ds.$$

Multiplying the integral times $\varepsilon^{-1/2}$ gives $\theta_5(x)$.

The boundary conditions $\mathcal{G}(w,0) = \mathcal{G}(w,1) = 0$

Next recalling the boundary conditions $\mathcal{G}(w,0) = \mathcal{G}(w,1) = 0$, we obtain, to leading order,

$$\begin{aligned} C_{a,0}(a + 2\sqrt{-\mu_{0,0}}) + C_{b,0}(a - 2\sqrt{-\mu_{0,0}}) &= 0, \\ C_{a,0}(a + 2\sqrt{\sigma_1 - \mu_{0,0}})e^{-\theta_5(1)} + C_{b,0}(a - 2\sqrt{\sigma_1 - \mu_{0,0}})e^{\theta_5(1)} &= 0, \end{aligned} \tag{9.20}$$

where we recall that $\sigma_1 = F(1)$. In order to find (9.21) we need to evaluate

$$\mathcal{G}(w,x) = w(x) - \frac{2\sqrt{\varepsilon}}{a} w_x(x),$$

where we write $w := w_{0,0}(x)$. Differentiating $w_{0,0}(x)$ we obtain

$$\begin{aligned} w_x(x) &= [F(x) - \mu_{0,0}]^{-1/4}[-\theta_5'(x) C_{a,0} e^{-\theta_5(x)} + \theta_5'(x) C_{b,0} e^{\theta_5(x)}] \\ &\quad -(1/4)[F(x)]'[F(x) - \mu_{0,0}]^{-5/4}[C_{a,0} e^{-\theta_5(x)} + C_{b,0} e^{\theta_5(x)}] \end{aligned}$$

where $\theta_5'(x) = \varepsilon^{-1/2} \frac{d}{dx} \int_0^x \sqrt{F(s) - \mu_{0,0}} ds = \sqrt{F(x) - \mu_{0,0}}$. Thus

$$\begin{aligned}\mathcal{G}(w,x) &= [F(x)-\mu_{0,0}]^{-1/4}[C_{a,0}e^{-\theta_5(x)}+C_{b,0}e^{\theta_5(x)}]\\ &\quad -\frac{2}{a}[F(x)-\mu_{0,0}]^{-1/4}[-\sqrt{F(x)-\mu_{0,0}}C_{a,0}e^{-\theta_5(x)}+\sqrt{F(x)-\mu_{0,0}}C_{b,0}e^{\theta_5(x)}].\end{aligned}$$

For $\mathcal{G}(w,0)=0$ we get

$$\mathcal{G}(w,0)=[\mu_{0,0}]^{-1/4}[C_{a,0}+C_{b,0}]-\frac{2}{a}[\mu_{0,0}]^{-1/4}[-\sqrt{\mu_{0,0}}C_{a,0}+\sqrt{\mu_{0,0}}C_{b,0}]=0.$$

Multiplying the above expression with $a[\mu_{0,0}]^{1/4}$ we get the first equation in (9.21).

For $\mathcal{G}(w,1)=0$ we get

$$\begin{aligned}\mathcal{G}(w,1) &= [\sigma_1-\mu_{0,0}]^{-1/4}[C_{a,0}e^{-\theta_5(1)}+C_{b,0}e^{\theta_5(1)}]\\ &\quad -\frac{2}{a}[\sigma_1-\mu_{0,0}]^{-1/4}[-\sqrt{\sigma_1-\mu_{0,0}}C_{a,0}e^{-\theta_5(1)}+\sqrt{\sigma_1-\mu_{0,0}}C_{b,0}e^{\theta_5(1)}]\\ &= 0.\end{aligned}$$

Multiplying the above equation with $a[\sigma_1-\mu_{0,0}]^{1/4}$ we get the second equation in (9.21).

The eigenvalue $\lambda_{0,0}$

Substituting

$$C_{b,0}=-C_{a,0}\frac{a+2\sqrt{-\mu_{0,0}}}{a-2\sqrt{-\mu_{0,0}}},$$

in the second equation in (9.22) we get

$$\left(-C_{a,0}\frac{a+2\sqrt{-\mu_{0,0}}}{a-2\sqrt{-\mu_{0,0}}}\right)(a+2\sqrt{\sigma_1-\mu_{0,0}})e^{-\theta_5(1)}+C_{b,0}(a-2\sqrt{\sigma_1-\mu_{0,0}})e^{\theta_5(1)}=0.$$

Here $\theta_5(1)\geq\mathcal{O}(\varepsilon^{-1/2})$, thus we must have that $a-2\sqrt{\sigma_1-\mu_{0,0}}=0$. Hence, we find to leading order that $\mu_{0,0}=F(1)-a^2/4$. Using (5.4) and (6.3) we find that

$$\lambda_{0,0}=f(1)-\ell. \tag{9.21}$$

The eigenfunction $w_{0,0}(x)$
We will now evaluate $w_{0,0}(x)$

$$w_{0,0}(x) = 2\Delta_5[F(x) - \mu_{0,0}]^{-1/4}\sinh(\Phi(x)), \quad x \in [0,1], \tag{9.22}$$

where

$$\Phi(x) = \frac{1}{\varepsilon^{1/2}}\int_0^x \sqrt{F(s) - \mu_{0,0}}ds - \frac{\mu_{0,1}}{2}\int_0^x \frac{1}{\sqrt{F(s) - \mu_{0,0}}}ds + \log\Delta_5,$$

$$\Delta_5^2 = \frac{\beta_1 + \sqrt{\beta_1^2 - 1}}{\beta_1 - \sqrt{\beta_1^2 - 1}}, \quad \beta_1 = \frac{a}{2\sqrt{F(1)}}.$$

We can write

$$C_{b,0} = -C_{a,0}\frac{a + 2\sqrt{-\mu_{0,0}}}{a - 2\sqrt{-\mu_{0,0}}} = -C_{a,0}\frac{\frac{a}{2\sqrt{\sigma_1}} + \frac{1}{\sqrt{\sigma_1}}\sqrt{a^2/4 - \sigma_1}}{\frac{a}{2\sqrt{\sigma_1}} - \frac{1}{\sqrt{\sigma_1}}\sqrt{a^2/4 - \sigma_1}} = -C_{a,0}\frac{\beta_1 + \sqrt{\beta_1^2 - 1}}{\beta_1 - \sqrt{\beta_1^2 - 1}},$$

thus $C_{b,0} = -C_{a,0}\Delta_5^2$. Substituting this in (9.23) we get

$$\begin{aligned} w_{0,0}(x) &= [F(x) - \mu_{0,0}]^{-1/4}(-C_{a,0})[e^{\theta_5(x) + \log\Delta_5^2} - e^{-\theta_5(x)}] \\ &= [F(x) - \mu_{0,0}]^{-1/4}(-C_{a,0})e^{(1/2)\log\Delta_5^2}\left[e^{\theta_5(x) + (1/2)\log\Delta_5^2} - e^{-(\theta_5(x) + (1/2)\log\Delta_5^2)}\right] \\ &= 2\Delta_5[F(x) - \mu_{0,0}]^{-1/4}\sinh(\Phi(x)), \end{aligned}$$

where $\Phi(x) = \theta_5(x) + \log\Delta_5$, and we have chosen $C_{a,0} = -1$. Recalling (6.1) we find

$$\omega_{0,0}(x) = 2\Delta_5[F(x) - \mu_{0,0}]^{-1/4}e^{ax/2\sqrt{\varepsilon}}\sinh(\Phi(x)), \quad \text{for } x \in [0,1].$$

9.2.2 The profiles for $a^2/4 > \sigma_U$

In this section we will study $\omega_{0,0}$ in (9.24) and the profiles for $a > 0$ and $a < 0$. First we insert the following parameters in $\omega_{0,0}$

$$\begin{aligned} \sigma_1 &= 0.1456 \\ \mu_{0,0} &= F(1) - a^2/4 \\ \mu_{0,1} &= -1 \\ \varepsilon &= 1 \cdot 10^{-4}. \end{aligned}$$

With these parameters $\omega_{0,0}(x)$ becomes

$$\omega_{0,0}(x) = 2\Delta_5 \left[F(x) + 0.000324\right]^{-1/4} \exp\left(\frac{ax}{2\sqrt{\varepsilon}}\right) \sinh\left(\Phi(x)\right),$$

where

$$\Phi(x) = \frac{1}{\varepsilon^{1/2}} \int_0^x \sqrt{F(s) + 0.000324}\, \mathrm{ds} + \frac{1}{2} \int_0^x \frac{1}{\sqrt{F(s) + 0.000324}} \mathrm{ds} + \ln(\Delta_5),$$

and

$$\Delta_5 = \frac{\left(\frac{a}{0.7632} + \sqrt{\frac{a^2}{0.5824} - 1}\right)^{1/2}}{\left(\frac{a}{0.7632} - \sqrt{\frac{a^2}{0.5824} - 1}\right)^{1/2}}.$$

Here $F(s)$ is defined as in section 9.1.3. Since $a^2/4 > \sigma_U$, we must choose $a < -0.7632$ for $a < 0$, and $a > 0.7632$ for $a > 0$.

The profile for $a > 0$ (or equivalently $\beta > 1$), sinking species

For $x \to 1$, the function $e^{ax/2\sqrt{\varepsilon}} \to \infty$ and is strictly increasing on $[0, 1]$. The function $\sinh(\Phi(x))$ is also strictly increasing on $[0, 1]$ and goes to infinity for $x \to 1$. Thus $\omega_{0,0}(x)$ corresponds to a BL (Figure 9.3).

The profile for $a < 0$ (or equivalently $\beta < -1$), buoyant species

The function has a maximum at

$$F(x) = a^2/4 + \mathcal{O}(\varepsilon^{1/2}).$$

The function $\omega_{0,0}$ takes on negative values in the beginning of the interval (Figure 9.4). Therefore we are not able to determine the structure of the phytoplankton pattern. Further research needs to be done in order to understand what happens with the phytoplankton population in this case.

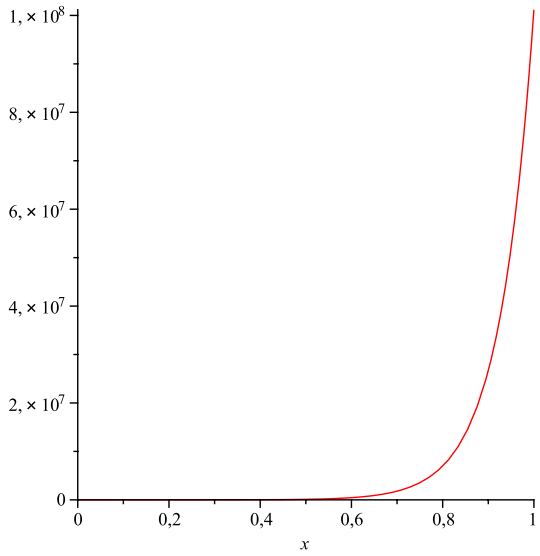

Figure 9.3: **Sinking species** The eigenfunction $\omega_{0,0}$ corresponds to a BL. Here $a = 0.765$, $\sigma_1 = 0.1456$, $\mu_{0,1} = -1$, and $\varepsilon = 1 \cdot 10^{-4}$.

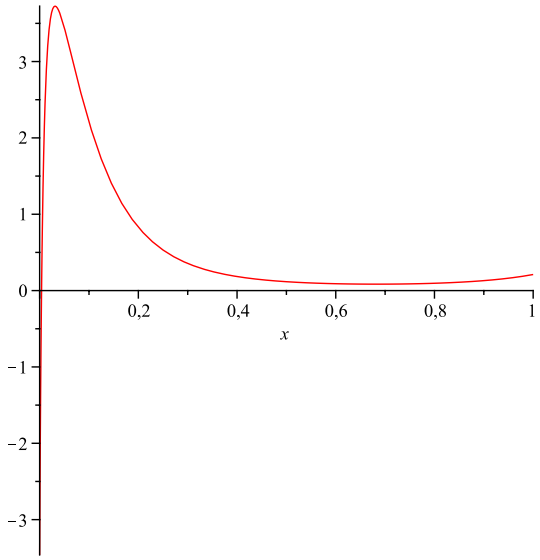

Figure 9.4: **Buoyant species** Because the eigenfunction $\omega_{0,0}$ has negative values in the beginning of the interval, the structure of the phytoplankton pattern can not be determined. Here, $a = -0.765$, $\sigma_1 = 0.1456$, $\mu_{0,1} = -1$, and $\varepsilon = 1 \cdot 10^{-4}$.

9.3 The transitional regime $\sigma_L < a^2/4 < \sigma_U$

Equations (9.13) and (9.22) may be used to derive information for the transitional regime $\sigma_L < a^2/4 < \sigma_U$. In particular, the transition between the case where λ_0 is associated with a spike (that is, with a DCM) occurs, to leading order, when $f(1) - \ell = \lambda^*$. Recalling (5.4) we rewrite this equation as

$$F(1) = f(0) - f(1) = a^2/4. \tag{9.23}$$

As mentioned in chapter 5, this condition reduces, to leading order,

(a) to $a^2/4 = \sigma_U$, for $0 < j_H \leq j_H^{(1)}$, and

(b) to $a^2/4 = \sigma_L$, for $j_H \geq j_H^{(2)}$.

For $j_H^{(1)} < j_H < j_H^{(2)}$ we have that $\sigma_U < a^2/4 < \sigma_L$.

Chapter 10

The Bifurcations

In this section we will identify the bifurcations the system (6.2) undergoes. We use the WKB expressions for the first few eigenvalues derived in chapter 9. In this way, we identify the regions in parameter space where the BL, DCM, and SL steady states become stable.

We are primarily interested in the effect of environmental conditions on phytoplankton. In particular, of nutrient concentration and diffusion. Therefore we choose to vary the parameters $\eta_H = N_H/N_B$ and $a = V/\sqrt{\mu D}$. The parameter η_H contains information about the nutrient levels and nutrient absorption by phytoplankton. The parameter a is a measure of diffusion. The remaining four dimensionless parameters ε, κ, j_H, and ℓ are kept constant. In this way our equations are simplified. For simplicity of presentation, we define the variables

$$\nu = (1+\eta_H)^{-1} \quad \text{and} \quad A = a^2/4.$$

The separating curves in the $(\nu, A)-$plane

The curves separating the regions in the $(\nu, A)-$plane (Fig. 10.1) are found by setting the expressions for λ_0 in (9.13) and (9.22) equal to zero, or equal to each other. In order to find these boundaries we must first recast (9.13) and (9.22) in terms of the rescaled parameters.

By setting the expression for λ_0 in (9.22) equal to 0, we obtain, to leading order, the vertical line separating the regions I, II, and III from the regions IV, V, and VI,

$$\nu = \ell(1 + \mathrm{e}^{\kappa} j_H).$$

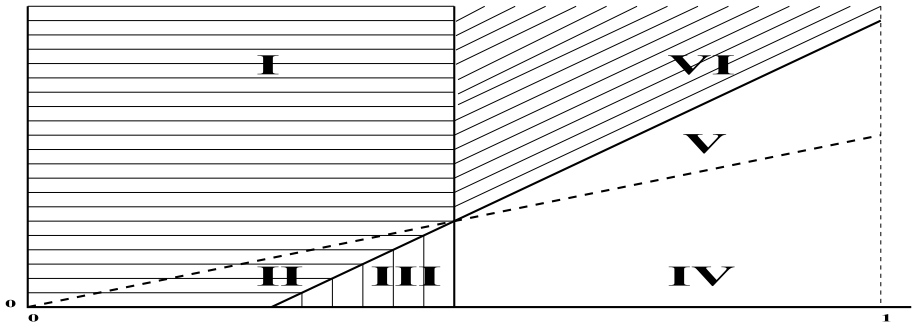

Figure 10.1: **Bifurcation diagram in the (ν, A)-plane.** The horizontal axis corresponds to $\nu = (1+\eta_H)^{-1}$, while the vertical one corresponds to $A = a^2/4$. **Sinking species.** In the region shaded horizontally, the trivial, zero state stable. In the region shaded vertically , DCMs bifurcate, while BLs remain damped. In the region shaded diagonally, BL profiles bifurcate, while DCM profiles remain damped. Finally in the unshaded region, both profiles grow linearly.
Buoyant species. In the region shaded horizontally, the trivial, zero state stable. In the region shaded vertically, SLs bifurcate. The uknown structure should be in the region shaded diagonally. Finally in the unshaded region, both profiles grow linearly.

Next, setting the expression for λ_0 in (9.13) equal to 0, we obtain, to leading order, the diagonal line separating the regions I, II, and IV from III, IV and V,

$$A = \frac{1}{1+j_H}\nu - \ell.$$

Setting the expressions for λ_0 in (9.13) and (9.22) equal to each other, we obtain the third line. This is the transitional regime (9.24),

$$A = \left(\frac{1}{1+j_H} - \frac{1}{1+\mathrm{e}^{\kappa} j_H}\right)\nu.$$

Now we can study the regions in Figure 10.1.

- **Regions I and II.**
  The eigenvalue λ_0 is given by (9.22) in region I, and by (9.13) ($n = 0$) in region II. In either case, $\lambda_0 < 0$, and hence the zero (trivial) state is stable. This means for sinking and buoyant species that the phytoplankton concentration is zero.

- **Region III.**
  The eigenvalue λ_0 is given by (9.13) and is positive. All the other eigenvalues are also positive.
  Sinking species: All of the eigenvalues are associated with DCMs for $a > 0$.
  Buoyant species: All of the eigenvalues are associated with SLs for $a < 0$.
  associated with DCMs for $a > 0$, and with SLs for $a < 0$.

- **Region VI.**
  The eigenvalue λ_0 is given by (9.22) and is positive. All the other eigenvalues are negative.
  Sinking species: The only bifurcation patterns in this regime are BL profiles for $a > 0$.
  Buoyant species: Since we do not know the structure of the phytoplankton pattern in this case for $a < 0$, we can give no further information for buoyant species in this regime.

- **Regions IV and V.**
  The eigenvalues associated with both BL and DCM profiles are positive in the case that $a < 0$. The eigenvalues associated with a SL and the unknown structure are also positive. Thus, no further information can be derived for the sinking and buoyant species from the linear analysis.

Since the physical region $\eta_H > 0$ corresponds to the region $0 < \nu < 1$, the formulas above imply that:

1. For $0 < \ell < (1 + \kappa j_H)^{-1}$:
   Both BL and DCM may bifurcate, for $a > 0$.
   A SL may bifurcate for $a < 0$.

2. For $0(1 + \mathrm{e}^{\kappa} j_H)^{-1} < \ell < (1 + j_H)^{-1}$:
   Only a DCM may bifurcate for $a > 0$, and only a SL may bifurcate for $a < 0$.

3. For $\ell > (1 + j_H)^{-1}$, the trivial state is stable.

Chapter 11

Assumptions and simplifications in the model

Limitations of the study in [17] and hence also in this study, arise from the assumptions and simplifications made in the phytoplankton-nutrient model. We will now state these assumptions and limitations.

Firstly, we have the one-dimensional assumption that considers variables only in the vertical direction. In more complex models one can include the possibility of horizontal flow and diffusion. This can be done by allowing W and N to vary with (x, y, z, t) and to include horizontal diffusion terms in (4.1). Although the horizontal gradients are not accounted for in the model, the linear stability analysis of the trivial state is essentially not influenced by this extension.

Specific formulas were assigned to the growth and light intensity functions $P(L, N)$ and $L(z, t)$, this is not essential for the analysis. Also the character of these functions is not essential for the analysis. One only needs that $f(x)$ is decreasing and bounded in $[0, 1]$.

The values of ε, a, and ℓ in (4.9) are typical of oceanic settings [10]. These values differ in estuary, and ε can no longer be assumed to be asymptotically small. Phytoplankton blooms in an estuary are strongly influenced by the concentration of suspended sediment and not only occur at a certain depth z, but also at a certain horizontal position in the estuary. Thus (4.13) must be extended to account for such blooms.

In [10], (4.1) was extended to a model for various phytoplankton species $W_i(z, t)$ $(i = 1, \ldots, n)$. A stability analysis of the trivial pattern $W_i \equiv 0$, $N \equiv N_B$ yields n uncoupled copies of (4.13), in which the parameters depend on the species,

i.e. on the index i. As a consequence, the results of [17] can also be applied to this setting where more than more species are present.

Chapter 12

Conclusion and Summary

We have analysed the model in [17] for $a < 0$ to determine the structure of the phytoplankton patterns exhibited by buoyant species. The results for buoyant species can be characterised as follows:

- If $a^2/4 < \sigma_L$ the phytoplankton pattern has the structure of a SL. For $a^2/4 > \sigma_U$ we were not able to determine the structure because the eigenfunction $\omega_{0,0}(x)$ in section 9.2.1 has negative values. Thus, for buoyant species, we are not able to predict for any given value of parameters what the structure of the phytoplankton pattern is. Future work could thus be undertaken to determine what this structure is. Since the structures of the phytoplankton patterns for buoyant species are different than the ones for sinking species, we can conclude from the results that the sign of the parameter a is very important in determining the structure of the phytoplankton pattern.
- Region VI in the bifurcation diagram in chapter 10 remains unknown. For buoyant species the trivial state $(\bar{\omega}, \bar{\eta})$ bifurcates into a SL or the structure that could not be determined. As for sinking species, also for buoyant species the regions V and VI remain unknown.
- Having studied all the mathematical analysis in [17] for sinking and buoyant species we can also conclude that all the theorems, lemmas, and defined functions in [17] are also valid for buoyant species. Despite not knowing the other structure, this is of great value, since now [17] can also be used for buoyant species. As already stated before, the mathematical analysis shows that the sign of the parameter a becomes relevant when studying the profiles and structures of the eigenfunctions in the chapters 8 en 9. In chapter 8, the profiles of the eigenfunctions for buoyant species are different than the ones of sinking species. In chapter 9 we have seen that the structures of the eigenfunctions for buoyant species are different than the ones for sinking species.

The findings of this study have highlighted the need for further research into modelling the dynamics of buoyant species. Although we were not able to determine the other structure, the results illustrate that sinking and buoyant species show different population dynamics. To obtain more insight in the dynamics of buoyant species further study of the eigenfunction $\omega_0(x)$ in section 8.1.1 and the function $\omega_{0,0}(x)$ in section 9.1.2 is necessary. Further research is needed to investigate why sinking and buoyant species are favoured in particular environments and how this might effect the patterns they form under certain conditions.

Appendix A

Airy functions

We summarize the expressions of the Airy functions Ai, Bi and their derivatives, which we will use repeatedly.

$$\begin{aligned} \mathrm{Ai}(z) &= (\pi^{-1/2} z^{-1/4}/2)\exp\left(-(2/3)z^{3/2}\right), \quad z \uparrow \infty, \\ \mathrm{Ai}'(z) &= -(\pi^{-1/2} z^{1/4}/2)\exp\left(-(2/3)z^{3/2}\right), \quad z \uparrow \infty. \end{aligned}$$

$$\begin{aligned} \mathrm{Bi}(z) &= (\pi^{-1/2} z^{-1/4})\exp\left((2/3)z^{3/2}\right), \quad z \uparrow \infty, \\ \mathrm{Bi}'(z) &= -(\pi^{-1/2} z^{1/4})\exp\left((2/3)z^{3/2}\right), \quad z \uparrow \infty. \end{aligned}$$

Lemma A.2. *The function* $\Gamma(\mathrm{Ai}, \bar{\chi})$ *defined in (5.3) has no positive roots. For any* $N \in \mathbf{N}$*, there is a* $\varepsilon_0 > 0$ *such that, for all* $0 < \varepsilon < \varepsilon_0$, $\Gamma(\mathrm{Ai}, \bar{\chi})$ *has roots* $A'_{N,\sigma} < \ldots < A'_{1,\sigma} < 0$ *satisfying*

$$|A'_{n,\sigma} - (A_n + \beta^{-1}\sqrt{\gamma})| < c_a \gamma \quad \textit{for some} \quad c_a < 0.$$

Here, $A_{n<0}$ is the *n-th root of* Ai*, see Fig. 5.1 and* β, γ *are given in (7.1). For* $\beta > 1$ (*equivalently, for* $0 < \sigma < a^2/4$,) *the function* $\Gamma(\mathrm{Bi}, \gamma^{-1}(\psi))$ *defined in (5.3) has a root* $B_{0,\sigma} > 0$ *satisfying*

$$|B_{0,\sigma} - (\beta^2 - 1 + 2\beta^{-1}\gamma^{3/2})| < c_b \gamma^3, \quad \textit{for some} \quad c_b > 0.$$

Proof. The fact that there exist no positive roots of $\Gamma(\mathrm{Ai}, \bar{\chi})$ is immediate by the fact that $\mathrm{Ai}(\bar{\chi}) > 0$ and $\mathrm{Ai}'(\bar{\chi}) < 0$ for all $\bar{\chi} > 0$.

Next, the existence of N discrete solutions may be proved in the following way. Let $|A_N| < X < |A_{N+1}|$ be fixed and $I_1, \ldots, I_N$ be disjoint intervals around $A_1, \ldots, A_N$, respectively. It is easy to prove that the function $\Gamma(\mathrm{Ai}, \bar{\chi})$ is $\mathcal{O}(\sqrt{\gamma})$ close to Ai over $[-X, 0]$ in the norm introduced in (7.10). Thus, for all $0 < \gamma < \gamma_0$ (with γ_0 small enough), $\Gamma(\mathrm{Ai}, \bar{\chi})$ has N distinct roots $A'_{1,\sigma} \in I_1, \ldots, A'_{N,\sigma} \in I_N$ in $[-X, 0]$. The fact that these are ordered as $A'_{N,\sigma} < \ldots < A'_{1,\sigma}$ follows from $A_{N,\sigma} < \ldots < A_{1,\sigma}$ and the fact that the intervals $I_1, \ldots, I_N$ were chosen to be disjoint. The bounds on $A'_{1,\sigma}, \ldots, A'_{N,\sigma}$ may be derived by writing $A'_{n,\sigma} = \sum_{\ell \geq 0} \varepsilon^{\ell/6} a^{(\ell)}_{n,\sigma}$ and substituting into the equation $\Gamma(\mathrm{Ai}, \bar{\chi}) = 0$.

The existence of $B_{0,\sigma} > 0$ and the bound on it may be established using the Airy functions and their derivatives. □

Appendix B

Proof of Lemma 4.2

Proof. Using definition (7.8), we calculate

$$\mathcal{A}\bar{\chi}) - \Gamma(\mathrm{Ai}, \bar{\chi}) = -\frac{\Gamma(\mathrm{Ai}, \gamma^{-1} + \bar{\chi})}{\Gamma(\mathrm{Bi}, \gamma^{-1} + \bar{\chi})}\Gamma(\mathrm{Bi}, \bar{\chi}).$$

To estimate the fraction in the right member, we apply standard theory for Airy functions, see [1]. Using the Airy functions and their derivatives from Appendix A, we find that

$$\sup_{[X,0]} \left| \exp\left(\frac{4}{3\gamma^{3/2}} + \frac{2\bar{\chi}}{\gamma^{1/2}}\right) \frac{\Gamma(\mathrm{Ai}, \gamma^{-1} + \bar{\chi})}{\Gamma(\mathrm{Bi}, \gamma^{-1} + \bar{\chi})} - \frac{1}{2}\frac{\beta+1}{\beta-1} \right| < c_1\sqrt{\gamma},$$

for some $c_1 > 0$ and γ small enough. Therefore,

$$\sup_{[X,0]} \left| \frac{\Gamma(\mathrm{Ai}, \gamma^{-1} + \bar{\chi})}{\Gamma(\mathrm{Bi}, \gamma^{-1} + \bar{\chi})} \right| < c_2 \exp\left(-\frac{4 + 6X\gamma}{3\gamma^{3/2}}\right),$$

for some $c_2 > 0$. Next, $\sup |\Gamma(\mathrm{Bi}, \bar{\chi})| \leq c_3$, for some $c_3 > 0$, since Bi and Bi$'$ are uniformly bounded over $[X, 0]$. Combining these estimates, we find

$$\sup_{[X,0]} |\mathcal{A}(\bar{\chi}) - \Gamma(\mathrm{Ai}, \bar{\chi})| < c_4 \exp\left(-\frac{4 + 6X\gamma}{3\gamma^{3/2}}\right),$$

for some $c_4 > 0$ and for all γ small enough.

Next we differentiate (B.1) and we calculate

$$\begin{aligned}\mathcal{A}'(\bar{\chi}) - \Gamma(\mathrm{Ai}_i', \bar{\chi}) &= \left(\frac{\Gamma(\mathrm{Ai}, \gamma^{-1}+\bar{\chi})\Gamma(\mathrm{Bi}', \gamma^{-1}+\bar{\chi})}{[\Gamma(\mathrm{Bi}, \gamma^{-1}+\bar{\chi})]^2} - \frac{\Gamma(\mathrm{Ai}', \gamma^{-1}+\bar{\chi})}{\Gamma(\mathrm{Bi}, \gamma^{-1}+\bar{\chi})}\right)\Gamma(\mathrm{Bi}, \bar{\chi}) \\ &\quad -\frac{\Gamma(\mathrm{Ai}, \gamma^{-1}+\bar{\chi})}{\Gamma(\mathrm{Bi}, \gamma^{-1}+\bar{\chi})}\Gamma(\mathrm{Bi}', \bar{\chi}).\end{aligned}$$

Using Appedix A, we may bound the term in parentheses by

$$\frac{c_1'}{\sqrt{\gamma}}\,\exp\left(-\frac{4+6X\gamma}{3}\left(\frac{1}{\gamma}\right)^{3/2}\right),$$

for some $c_1' > 0$. Next, $\Gamma(\mathrm{Bi}, \bar{\chi})$ was uniformly bounded by a constant c_3 above. Also, the term $\Gamma(\mathrm{Bi}', \bar{\chi})$ may be bounded by a constant c_3', since

$$\Gamma(\mathrm{Bi}', \bar{\chi}) = \mathrm{Bi}'(\bar{\chi}) - \beta\sqrt{\gamma}\mathrm{Bi}''(\bar{\chi}) = \mathrm{Bi}'(\bar{\chi}) - \beta\sqrt{\gamma}\bar{\chi}\mathrm{Bi}(\bar{\chi}),$$

and the term multiplying it was bound (B.2). These inequalities yield, then,

$$\|\mathcal{A}'(\bar{\chi}) - \mathrm{A'}_i(\bar{\chi})\|_{[X,0]} < c_2'\gamma^{-1/2}\exp\left(-\frac{4+6X\gamma}{3\gamma^{3/2}}\right),$$

for some $c_2' > 0$ and for all γ small enough. Equation (7.11) follows now from (B.3) and (B.4).

□

Appendix C

Proof of Lemma 4.3

Proof. Definition (7.9) yields

$$\mathcal{B}(\gamma^{-1}\bar{\psi}) - \Gamma(\mathrm{Bi}, \gamma^{-1}(1+\psi)) = -\frac{\Gamma(\mathrm{Bi}, \gamma^{-1}\bar{\psi})}{\Gamma(\mathrm{Ai}, \gamma^{-1}\bar{\psi})}\Gamma(\mathrm{Ai}, \gamma^{-1}(1+\bar{\psi})).$$

To estimate the right member, we work as in Appendix B. Using Appendix A, the Airy functions and their derivatives, we obtain

$$\sup_{[\Psi_R, \Psi_L]} \left| E(\gamma^{-1}(1+\bar{\psi}))\frac{\Gamma(\mathrm{Bi}, \gamma^{-1}\bar{\psi})}{\Gamma(\mathrm{Ai}, \gamma^{-1}\bar{\psi})}\Gamma(\mathrm{Ai}, \gamma^{-1}(1+\psi)) \right| < c_1\gamma^{1/4}\left[\frac{E(\gamma^{-1}(1+\Psi_L))}{E(\gamma^{-1}\Psi_L)}\right]^2,$$

for some $c_1 > 0$ and γ small enough.

Next, differentiating (C.1), we calculate

$$\begin{aligned}\mathcal{B}'(\gamma^{-1}\bar{\psi}) - \Gamma'(\mathrm{Bi}, \gamma^{-1}(1+\bar{\psi})) &= -\frac{\Gamma(\mathrm{Bi}, \gamma^{-1}\bar{\psi})}{\Gamma(\mathrm{Ai}, \gamma^{-1}\bar{\psi})}\Gamma(\mathrm{Ai}', \gamma^{-1}(1+\bar{\psi})) \\ &\quad + \left(\frac{\Gamma(\mathrm{Bi}, \gamma^{-1}\bar{\psi})\Gamma(\mathrm{Ai}', \gamma^{-1}\bar{\psi})}{\left[\Gamma(\mathrm{Ai}, \gamma^{-1}\bar{\psi})\right]^2} - \frac{\Gamma(\mathrm{Bi}', \gamma^{-1}\bar{\psi})}{\Gamma(\mathrm{Ai}, \gamma^{-1}\bar{\psi})}\right)\Gamma(\mathrm{Ai}, \gamma^{-1}(1+\bar{\psi})).\end{aligned}$$

Using Appendix A to estimate the right member, we find

$$\sup_{[\Psi_R, \Psi_L]} \left| E(\gamma^{-1}(1+\bar{\psi}))\left[\mathcal{B}'(\gamma^{-1}\bar{\psi}) - \Gamma'(\mathcal{B}\rangle, \gamma^{-1}(1+\bar{\psi}))\right] \right| < c_1'\gamma^{-1/4}\left[\frac{E(\gamma^{-1}(1+\Psi_L))}{E(\gamma^{-1}\Psi_L)}\right]^2,$$

for some $c_1' > 0$ and γ small enough.

The desired result follows from (C.2) and (C.3). □

Bibliography

[1] Bender, C.M. and Orszag, S.A.(1999). *Advanced Mathematical Methods for Scientists and Engineers.* Applied Mathematical Sciences **35**,Springer-Verlag.

[2] Camacho, A.(2006).On the occurrence and ecological features of deep chlorophyll maxima (DCM) in Spanish ratified lakes.*Limnetica.* 25(1-2),453-478.

[3] Cockell, C., Corfield, R., Edwards, N., Harris, N.(2007). *An introduction to the Earth-Life System.*Cambridge University Press.

[4] Ebert,U., Arrays,M., Temme, N., Sommeijer, B.P., Huisman, J. (2001).Critical conditions for phytoplankton blooms. *Bull.Math.Biology.***63**(6), 1095-1124.

[5] Falkowski, P.G. (2002).The Ocean's Invisible Forest.*Scientific American.*

[6] Fasham, M.J.R.(2003).*Ocean Biogeochemistry.*Springer-Verlag,Berlin Heidelberg.

[7] Fennel, W. and Neumann (2004),T. *Introduction to the Modelling of Marine Ecosystems*, Elsevier B.V.

[8] Gray, J.S. and Elliott, M.(2009).*Ecology of Marine Sediments.*Oxford University Press.

[9] Huisman, J., Arrayas,M., Ebert, U., and Sommeijer, B. (2003).How do sinking phytoplankton species manage to persist?*Am. Naturalist* **159**, 245-254.

[10] Huisman, J., Pham Ti, N. N., Karl,D. M., and Sommeijer, B. P. (2006). Reduced mixing generates oscillations and chaos in the oceanic deep chlorophyll maximum. *Nature.* **439**, 322-325.

[11] Huisman, J., Ebert,U., Arrayas,M., Temme,N., and Sommeijer,B. (2001). Critical conditions for phytoplankton blooms, *Bull. Math. Biol.* **63** 1095-1124.

[12] Huisman,J., van Oostveen, P., and Weissing, F.J. (1999). Critical depth and critical turbulence: Two different mechanisms for the development of phytoplankton blooms. *Limnol.Oceanogr.***44**(7), 1781-1787.

[13] Holmes, M.H. (1995).*Introduction to Perturbation Methods.*Texts in Applied Mathematics **20**, Springer-Verlag.

[14] Klausmeier, C.A. and Lichtman, E. (2001). Algal games: The vertical distribution of phytoplankton in poorly mixed water columns. *Limnol. Oceanogr.***46**(8),1998-2007.

[15] Lalli, C.M. and Parsons, T.R.(?). *Biological Oceanography an Introduction*, Elsevier.

[16] Reynolds, C. (2006). *Ecology of Phytoplankton*, Cambridge: Cambridge University Press.

[17] Zagaris, A., Doelman,A., Pham Thi,N.N. and Sommeijer, B.P.(2009). Blooming in a non-local, coupled phytoplankton-nutrient model. *Siam journal of Applied Sciences.* **69**(4), 1174-1204

Acknowledgments

First and foremost I owe my deepest gratitude to my supervisor Dr. Vivi Rottschäfer. I am very grateful for her knowledge, patience and effort. Her guidance and support from the initial to the final level enabled me to develop an understanding of the subject. I offer my regards to all the teachers, professors and students who have taught me mathematics and supported me in any respect during my study of mathematics. I am especially grateful to Dr. Robert-Jan Kooman for teaching me patiently the theory of mathematical physics. I am also heartily thankful for Jan Vanderschoot for helping me with the layout of my thesis. Lastly, and most importantly, I wish to thank my parents, Lucian Veselic and Maud Veselic Charvat. They have always provided a loving environment for me, supported me, taught me, and loved me. They have helped through difficult times and without them I could not have completed my thesis. I dedicate my thesis to them.